Acta Geochim (2023) 42:1079–1103
https://doi.org/10.1007/s11631-023-00636-4

ORIGINAL ARTICLE

Correlations between trace elements in pyrite and gold mineralization of gold deposits on the North China platform

Jianzhao Yin[1,2] · Ying Sun[3] · Haoyu Yin[4] · Hongyun Shi[5] · James Sparling[6] · Yuhong Chao[7] · Shoupu Xiang[8]

Received: 17 February 2023 / Revised: 2 August 2023 / Accepted: 17 August 2023 / Published online: 28 August 2023

Abstract By studying both the microscopic physical and chemical typomorphic characteristics of typical mineral pyrite samples associated with representative gold deposits on the north-central margin of the North China Platform, this paper seeks to identify macroscopic metallogenic mechanisms of gold deposits and to reveal the formation mechanism of lattice gold in pyrite. Typomorphic characteristics of pyrite reveal that pyrite grain size has a negative correlation with gold content. Cubic pyrite, as the dominant crystal form, contains more gold than pentagonal dodecahedral pyrite. Both pyrite crystal forms and chemical compositions indicate that the replacement style of gold deposit formed in a low saturability, low sulfur fugacity, and at temperatures either much higher or much lower than its best forming temperature; comparatively, that of the quartz vein style of gold deposit occurred under conditions with the best temperature, rich in sulfur, and with high sulfur fugacity. The Au/Ag ratios of the pyrites show that both the replacement and quartz vein styles of deposits are mesothermal and hypothermal, while the Co/Ni ratios of the pyrites indicate that the quartz vein style is of magmatic-hydrothermal origin. The X-ray diffraction intensity of pyrite rich in gold is lower than that of pyrite poor in gold at the quartz vein style. In general, with an increase in gold content in pyrite, the total sum intensity ΣI decreases. The pyroelectricity coefficient has a negative correlation trend with the values of (Co + Ni + Se + Te)-As and (Co + Ni + Se + Te)/As. The pyrite pyroelectricity of the replacement style is N-type, indicating that it formed under low sulfur fugacity, while that of the quartz vein style is a mixture of P-N types, indicating that it formed under high sulfur fugacity. On the pyroelectricity-

✉ Jianzhao Yin
jzyin7@jlu.edu.cn

Ying Sun
sunying7@jlu.edu.cn

Haoyu Yin
yinhaoyu11@163.com

Hongyun Shi
hongyunshi@yahoo.com

James Sparling
james.sparling@hocplc.com

Yuhong Chao
435975944@qq.com

Shoupu Xiang
shoupux@163.com

[1] College of Earth Sciences, Jilin University, Changchun 130061, China

[2] Wuhan Institute of Technology, Wuhan 430074, China

[3] College of Geoexploration Science and Technology, Jilin University, Changchun 130062, China

[4] Guinea Westfield Mining Company-Sarlu, Jinzhong 031300, China

[5] Orient Resources Ltd., Richmond, BC V7A 4V5, Canada

[6] Hochschild Mining Canada Corp., Suite 1700 Park Place, 666 Burrard Street, Vancouver, BC V6C 2X8, Canada

[7] Ganzhongnan Institute of Geology and Mineral Exploration, 658 Jiefangxilu Road, Nanchang 330002, China

[8] Silvercorp Metals Inc., Suite 601-Building 1, China View Mansion, #A2 East GongTi Road, Chaoyang District, Beijing 100027, China

temperature diagram, pyrite of the replacement style is mainly distributed between 200 and 270 °C, while that of the quartz vein style varies between 90–118 and 274–386 °C, demonstrating a multistage forming process. In contrast to previous researchers' conclusions, the authors confirm the existence of lattice gold in pyrites through the use of an electron paramagnetic resonance (EPR) test. Au in the form of Au^{+}, entering pyrite as an isomorph and producing electron–hole centers, makes the centers produce spin resonance absorption and results in EPR absorption peak II. The intensity of auriferous pyrite absorption peak II has certain direct positive correlations with pyrite gold content. The #I and #III absorption peaks of pyrites possibly result from the existence of Ni^{2+} and/or Cu^{2+}. γ_1, γ_2, and γ_3 are the strongest and most typical absorption peaks of the infrared spectra of the pyrites. Generally, with the increase in gold content in the pyrite samples, γ_1, γ_2, and γ_3 tend to shift to higher wavenumbers, and the gold content in the pyrite samples has a positive correlation with their relative absorbance.

Keywords Unit cell parameter · Pyroelectricity · Electron paramagnetic resonance · Infrared spectrum · Pyrite · Gold deposit

1 Introduction

As is typically commonplace, gold can occur in nature as free gold and/or as various alloys by forming a complete series of solid solutions with other metals including silver, platinum metals, and so on (Jones and Fleischer 1969). Generally, native gold occurs in hard rock minerals via four forms including lattice gold in other minerals mainly including pyrite and quartz (Dang 1991; Hu 1993; Yin and Shi 1995; Liu 1997; Yin et al. 2021). Very limited research has been done on lattice gold in other minerals, although numerous studies have been done on free gold occurring as inclusions, in fractures, and between crystals of other minerals (Dang 1991; Hu 1993; Yin and Shi 1995; Wang and Chen 1996; Liu 1997; Yin et al. 2021).

The authors of this paper confirm that there is lattice gold available in pyrite, the most common gold-bearing mineral in almost all of the gold deposits in the world. Meanwhile, we seek to reveal the mechanisms of gold mineralization in detail by studying both the physical and chemical characteristics of pyrite from representative gold deposits on the North China platform.

By observing and studying the microscopic world through the dominant gold-bearing mineral pyrite, the subject of this paper, which was collected from the representative gold deposits in the study area, the authors try to reveal the metallogenic gold ore-forming process. To some extent, the study of this article will help with gold mineral prospection, evaluation, and gold mineralization studies of related deposits. More importantly, this study will possibly provide a solid basis for metallurgical technology of gold ores with lattice gold and thus improve the metallurgical recovery of this kind of gold ore worldwide.

2 Regional geology

Northwestern Hebei Province, the study area of this paper, is located in the convergent part between the Inner Mongolian axis and the Yanshan folding zone of the North China platform. Most of the over 100 lode gold deposits in the region are located within a triangular area among the Xuanhua, Checheng, and Chongli towns and are thus called a gold triangle with an area of 1500 km^2 (Fig. 1, Yin and Shi 1995; Yin et al. 2021).

According to the previous researchers (Zhang 1984; Song et al. 1994; Xu et al. 2014; Chao et al. 2022a, b; Wang et al. 2022), strata within the study area are composed of the following tectostratigraphic units, namely, the Archean Sanggan Group metamorphic basement consisting of dark-colored granulite, plagioclase hornblende gneiss, and migmatite, which are also the major host rocks of both the replacement and quartz vein styles of gold deposits; the Middle Proterozoic Changcheng Group marine facies of sedimentary cover; the Mesozoic continental facies of volcanic-sedimentary rocks; and the Cenozoic sedimentary overburden (Fig. 1).

Generally, the Archean metamorphic basement mentioned above experienced three phases of folding and formed the EW hinge synclinorium, the overturned NNW-NWW hinge synclinorium, and the NW-NWW hinge synclinorium respectively, while the well-developed faults include EW-, NW- and NE-striking faults. Of these, the EW-striking Chongli-Checheng giant fault plays an important role in the formation of gold deposits. Igneous rocks including ultrabasic, basic, intermediate, acidic, and alkali intrusive rocks, are well developed and mainly formed in the following tectonomagmatic cycles: the Archean gneissic granite, diorite and hornblende diopsidite; the Early Proterozoic peridotite, pyrolite and dunite; various granites, alkaline complex intrusive rocks and ultrabasic rocks of the Hercynian orogeny; and the widespread distributed granite of the Mesozoic Yanshan orogeny. Numerous different kinds of dikes are well developed in the area (Song et al. 1994; Yin and Shi 1995; Xu et al. 2014; Yin et al. 2021; Chao et al. 2022b).

There exist three gold mineralization styles in the region, namely, quartz vein style, replacement style, and alkali complex intrusion-related style. The replacement style of gold mineralization is a mineralization type formed

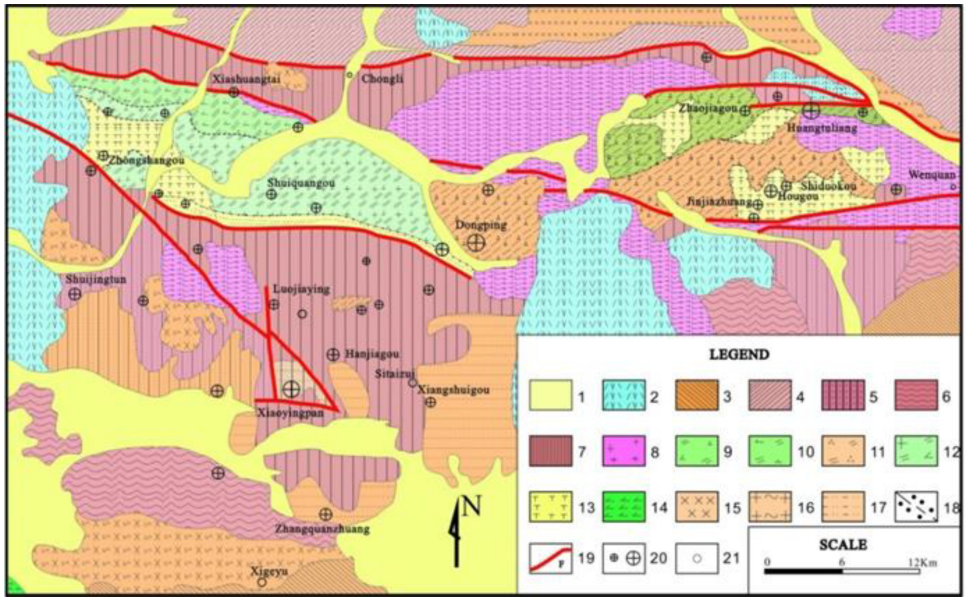

Fig. 1 Simplified geological map of the gold deposits in the study area (after Yin et al. 1995, 2021a). 1. Quaternary sediments; 2. Tuff conglomerate, sandstone and breccia of the Upper Jurassic system; 3. Sandstone, siltstone and dolomite of the Proterozoic Changcheng system; 4. Metamorphic granulite of the Late Archean Hongqiyingzi Group; 5. Metamorphic granulite of the Aijiagou Formation of the Archean Sanggan Group; 6. Gneiss of the Shuidizhuang Formation of the Archean Sanggan Group; 7. Metamorphic granulite of the Jiagouhe Formation of the Archean Sanggan Group; 8. Granite of the Yanshan orogeny; 9. Amphibolite monzonite of the Hercynian orogeny; 10. Pyroxene amphibolite monzonite of the Hercynian orogeny; 11. Quartz monzonite of the Hercynian orogeny; 12. Amphibolite adamellite of the Hercynian orogeny; 13. Syenite of the Hercynian orogeny; 14. Pyroxenite of the Hercynian orogeny; 15. The Proterozoic granite-gneiss; 16. The Archean granite-gneiss; 17. The Archean metamorphic mica quartz diorite; 18. Marginal migmatization zone of the monzonite; 19. Fault and/or fault zone; 20. Small to large size gold deposits; 21. Town and/or village

by gold-bearing pyrite and/or quartz replacing carbonate minerals in the country rocks (Roberts 1986; Percival et al. 1990; Sillitoe and Bonham 1990; Adams and Putnam III 1992; Garwin et al. 1995; Arehart 1996; Barton et al. 1997; Lobato and Vieira 1998; Poulsen et al. 2000; Kingston 2009; Ravenelle 2013; Sillitoe 2020; Valette et al. 2020; Azzaman et al. 2021). The ore consists mainly of potassium feldspar, magnetite, specularite, quartz, pyrite, galena, chalcopyrite, bornite, native gold, electrum, tetrahedrite, calaverite, ankerite, calcite, barite, hematite, and malachite (Wang 1986; Zheng 1990; Gao 1991; Yin and Zhai 1994; Yin and Shi 1995; Yin et al. 2021; Chao et al. 2022b).

3 Mine geology

3.1 Xiaoyingpan gold mine

The Xiaoyingpan gold deposit is a mixed gold mineralization type dominated by replacement style and supplemented by quartz vein mineralization style. The ore body is generally 2.0–5.0 m thick, with a maximum thickness of 21.0 m. Individual ore bodies mainly appear in layer-like, lentils, and lenticular shapes. The main mineral assemblage includes native gold, electrum, calaverite, argentite, pyrite, chalcopyrite, galena, carinthite, specularite, malachite, limonite, hematite, quartz, calcite, potassium feldspar, chlorite, and sericite, etc. Ore texture and structure include disseminated, massive, semi-massive, replacement remnant and pseudomorphic, euhedral-heteromorphic granular, fragmented structure, etc.

The formation of the Xiaoyingpan gold deposit was the result of the multi-stage paragenetic process and has gone through the following paragenetic stages, namely (from early to late): Potassium feldspar-quartz compound vein stage (KF-Q_1)-Milky white quartz vein stage (Q_2)-Polymetallic sulfide-smoky quartz i.e., Replacement stage (R_3)-Carbonate mineral stage (C_4)-Supergene stage (S5). Among them, the third stage, that is, the replacement stage (R3), is the most important mineralization stage, marking the climax of the gold mineralization of the deposit (Yin and Shi 1995).

3.2 Zhangquanzhuang gold mine

As a sulfide-rich gold deposit, Zhangquanzhuang gold deposit is a typical quartz vein style mineralization. The ore body is generally 0.2–2.0 m thick and 10.0–2200.0 m long. The main mineral assemblages include native gold, electrum, pyrite, chalcopyrite, galena, ilmenite, quartz, potassium feldspar, iron dolomite, calcite, chlorite, epidote, sericite, etc. The ore structure and texture include vein, stockwork, agglomerate, dissemination, euhedral-heteromorphic granular, replacement remnant and pseudomorphic, dissolution and fragmentation, etc.

The formation of Zhangquanzhuang gold deposit consists of the following three metallogenic stages, namely (from early to late): Milky white quartz vein stage (Q1)-Smoky gray quartz-polymetallic sulfide stage (Q2), and Carbonate mineral stage (C3). Among them, the second stage, that is, the Smoky gray quartz-polymetallic sulfide stage (Q2), is the most important paragenetic stage, marking the climax of the gold mineralization of the deposit (Yin and Shi 1995).

3.3 Dongping gold mine

The Dongping gold deposit is an alkali complex intrusion-related style of gold mineralization discovered in the alkaline complex in the 1980s. The ore is sulfide-poor and telluride-rich type. The ore minerals of the Dongping gold deposit include native gold, pyrite, chalcopyrite, galena, magnetite, hematite, limonite, bornite, pyrrhotite, and telluride, etc. The main mineral assemblage is pyrite-chalcopyrite-various telluride-native gold-calaverite-hessite. Gangue minerals are mainly potassium feldspar, plagioclase, quartz, calcite, chlorite, epidote, zoisite, and sericite, with trace apatite, sphene, zircon, and so on. The ore texture mainly includes euhedral-semihedral crystal, metasomatic erosion, embedded crystal, fragmentation, interstitial, etc. The ore structure mainly includes patchy, mass, strip, veinlet, stockwork, breccia, geode, comb, honeycomb, and so on.

The formation of the Dongping gold deposit was the result of the multi-stage paragenetic process. Specifically, the formation of the Dongping gold deposit has gone through the following four paragenetic stages, namely (from early to late): Milky white quartz (Q_1)-potassium feldspar (K_1)-coarse-grained pyrite (cgPy) stage, Grey white quartz (Q_2)-brick-red potassium feldspar (K_2) stage, Potassium feldspar (K_3)-quartz (Q_3)-polymetallic sulfide stage, and Calcite-chert (Q_4)-barite stage. Among them, the third stage, that is, the Potassium feldspar (K_3)-quartz (Q_3)-polymetallic sulfide stage, is the most important paragenetic stage, marking the climax of the gold mineralization of the deposit (Yin and Shi 1995; Chao et al. 2022b).

4 Analytical methodology

Pyrite is one of the most common auriferous minerals in both the study area and any other gold deposits worldwide. With the addition of gold, the characteristics of pyrite will surely change. As a result, the mineralization mechanism of lode gold deposits can be revealed by studying these microscopic alterations. Most if not all of the pyrite samples, which formed in the dominant paragenetic stages as mentioned above, were collected from proper locations of the typical ore bodies of the selected representative large gold deposits in the study area.

Gold was analyzed through standard fire assay procedures. A weighed sample (30 g for FA430 and 50 g for FA450) was mixed with fire assay fluxes (borax, soda ash, silica, and litharge), and Ag was added for inquartation. The mixture was placed in a crucible to produce a fluid slag at 1000 °C. The crucible was then removed from the assay furnace, and the molten charge was carefully poured from the crucible into a mold allowing the slag to separate, leaving a lead button at its base. After cooling, the lead button was placed in a preheated cupel, which absorbed the lead when cupelled at 950 °C to recover the silver + gold (doré bead). Gold was then separated from the silver in the doré bead by parting with nitric acid. The remaining precious metal beads (gold) were weighed gravimetrically on a microbalance, dissolved in acid, and analyzed by atomic absorption (AA) spectrophotometry. During the fire assay, a commercial gold standard was inserted as QA/QC.

Silver and other trace elements were determined by a Thermo Scientific ICP Spectrometer—iCAP6000 after full acid digestion. During the ICP analysis, an internal standard pyrite sample was used as a reference. Assays of the standard and reference are reported in Table 2 along with the sample assays.

Electron paramagnetic resonance (EPR) measurements of the pyrites were performed at the EPR lab of the Department of Physics, Peking University, China. The test conditions were as follows: equipment used: BRUKER ER200D-SRC, temperature: 295 K, microwave frequency: 9.744–9.779 GHz, microwave power: 10 mW, scanned area: ± 2500 G, scanning time: 500 s, rated magnetic field: 5000 G, home position: 2500 G, modulation amplitude: 3.2 G.

5 Physical characteristics

Generally, pyrites of the three representative gold deposits, namely, the Xiaoyingpan, Zhangquanzhuang, and Dongping gold mines in the area, each formed in the following three mineralization stages and have different characteristics:

Pyrite of the early stage: coarse-grained (> 2 mm), perfect euhedral and/or subhedral crystal, disseminated in quartz and/or potassium feldspar-quartz veins/veinlets; gold content in this kind of pyrite is low and usually 1–17 g/t.

Pyrite of the middle stage: the dominant gold paragenetic stage of the gold deposits, light yellow to yellowish green, fine-medium grained (< 2 mm), allotriomorphic crystal, in the form of pellets and/or fine veinlets occurring in smoky quartz veins/veinlets; gold content in this kind of pyrite is usually 59–257 g/t.

Pyrite of the late stage: formed in the ending mineralization stage, namely, the carbonate stage of the gold deposits, mainly fine-grained (< 1 mm) dissemination in carbonate veins/veinlets with very low gold grade.

The general mineralogical characteristics of pyrites from the early and middle paragenetic stages of the Xiaoyingpan and Zhangquanzhuang gold mines, which are the subject of this paper, are summarized in Table 1.

Pyrite's crystal form reflects its forming conditions. For example, the (100) pyrite crystal occurs in low saturability, low sulfur fugacity, and at a temperature either much higher or much lower than pyrite's best forming temperature, while (210) pyrite crystal forms in an environment rich in sulfur and with high sulfur fugacity (Jin and Li 1985; Chen 1987). According to Table 1, it can be preliminarily concluded that pyrites from the Xiaoyingpan gold deposit formed in a low saturability, low sulfur fugacity environment and at temperatures either much higher or much lower than its best forming temperature, while that of the Zhangquanzhuang gold deposit occurred under conditions with the optimal temperature, rich in sulfur and with high sulfur fugacity (Jin and Li 1985; Chen 1987).

Pyrite grain size and gold content: Trace element analysis results of pyrites from both the Xiaoyingpan and Zhangquanzhuang gold deposits in Table 2 indicate that the grain size of pyrite has a negative correlation with its gold content: coarse-grained euhedral pyrite has a lower gold content than fine-grained subhedral and/or allotriomorphic pyrite (Fig. 2).

Pyrite crystal form and gold content: Electron microprobe measurements of pyrite show that cubic pyrite, as the dominant crystal form in the study area, contains more gold than pentagonal dodecahedron pyrite in the area (Table 3). This is different from the conclusions published by other researchers (Dong 1989; Hu et al. 1990; Xiang 1991; Li 1992).

6 Chemical characteristics

6.1 Major element compositions

Theoretically, the S and Fe contents of pyrite are 53.45% and 46.55%, respectively, and their standard mass ratio is S/Fe = 1.148 (Jin and Li 1985; Chen 1987). According to Table 3, the S/Fe ratio of pyrites from the Xiaoyingpan gold deposit is close to but slightly higher than the standard ratio, while that of most pyrites from the Zhangquanzhuang gold deposit is higher than the theoretical ratio (Fig. 3), showing a loss in Fe but a surplus in S, which is similar to the conclusion that the Zhangquanzhuang gold deposit occurred under conditions with the best conditions for the formation of pyrites.

6.2 Trace compositions

Au and Ag contents in pyrite from both Xiaoyingpan (Au = 1.11–5050 g/t and Ag = 4.4–750 g/t) and Zhangquanzhuang (Au = 5.22–3490 g/t and Ag = 41–1100 g/t) deposits vary between a very wide range (Tables 2, 3), reflecting that pyrites from these deposits formed in multistage metallogenic processes with nonuniform gold distributions. The average Au/Ag ratio of the Xiaoyingpan deposit is 3.29 and that of Zhangquanzhuang is 5.07 (Table 3 and Figs. 3, 4). According to Shao (1990), the Au/Ag ratio of pyrites from mesothermal and hypothermal gold deposits is usually over 1.0. This means that both the Xiaoyingpan and Zhangquanzhuang deposits are of mesothermal and hypothermal origin.

Copper, Pb, and Zn contents in the pyrites are relatively high in the area (Tables 2, 3, Fig. 5). This can be used as one of the gold ore-hunting indicators.

The Co/Ni ratio in pyrites from Xiaoyingpan, Shuijingtun, and Hanjiggou, the replacement style of gold deposits, is essentially below 1.0 (Tables 2, 3, Fig. 4); that of Zhangquanzhuang and Jinjiagou, the quartz vein style of gold deposits, is over 1.0; and that of Hougou, which is the same style as the Dongping large deposit, the alkaline complex intrusive rock-related style of gold deposits, is below 1.0. The three styles of gold deposits represent three gold metallogenic series in the area (Yin and Zhai 1994; Yin et al. 2021). According to Jin and Li (1985), the Co/Ni ratio in pyrites from magmatic-hydrothermal gold deposits is over 1.0, while that of other styles of gold deposits is below 1.0. As a result of this, the quartz vein style of gold deposit in the study area would be of magmatic-hydrothermal origin, while both the replacement and alkaline intrusive rock-related styles are not. Additionally, according to Tables 2 and 3, the Co/Ni ratios in pyrite of all three styles of gold deposits generally have a negative correlation with gold content; Jin and Li (1985) thought that this meant ore-forming materials were abyssal.

Se/Te and S/Se ratios in pyrites can provide genetic information, and those of magmatic-hydrothermal gold deposits are 9000–13000 and 5.0 (Chen 1987), respectively. The Se/Te and S/Se ratios in pyrites from both the Xiaoyingpan and Zhangquanzhuang gold deposits in

Table 1 General characteristics of pyrites from representative gold mines

Characteristics of pyrite		Gold mine			
		Xiaoyingpan		Zhangquanzhuang	
Paragenetic stage		The early stage	The late stage	The early stage	The late stage
Crystal form					
Cube		30%	60–70%	20%	55%
Pentagonal dodecahedron		–	< 5%	< 5%	20%
Other		–	–	–	< 1% (octahedron + dodecahedron)
Crystal size					
Coarse grained cube	> 5mm	5%	< 1%	< 5%	< 1%
	3-5mm	10%	5%	5%	< 5%
	1-3mm	10%	10%	10%	10%
Fine-grained cube	0.1–1.0mm	3–5%	35%	5%	35%
Pentagonal dodecahedron	< 0.1mm	< 1%	20%	< 5%	25%
Fractured degree					
Coarse grained		Very strong	Strong	Strong	Medium
Fine-grained		Strong	Medium	Medium	Weak
Style					
		Mainly dissemination with some cg clot	Dissemination, clot and fine veinlet	Clot, fine veinlet and Ds	Ds, clot and fine veinlet
Associated mineral					
		Milky white Q, K-feldspar, Cpy, Ga, native gold, specularite and limonite	Smoky Q, Ga, Spl, Cpy, Bn, Tt, altaite, native gold and electrum	Milky white to grey Q, Ga, Cpy and native gold	Smoky Q, Ga, Spl, Cpy, Bn, calcite, ankerite, native gold, and electrum
Secondary alteration					
		Strong limonite alteration dissolution along fractures and at margins of pyrite	Limonite alteration and dissolution exist	Strong dissolution	Weak dissolution
Gold-bearing potential					
Coarse grained		Poor	Good	Fair	Good
Fine-grained		Fair	Very good	Fair	Very good

cg, Coarse grained; fg, Fine grained; Ds, Dissemination; K, Potassium; Q, Quartz; Cpy, Chalcopyrite; Ga, Galena; Spl, Sphalerite; Bn, Bornite; Tt, Tetrahedrite

Table 3 are comparably lower (Fig. 3), indicating that both have nothing to do with magmatic-hydrothermal solutions. The Zhangquanzhuang style of gold deposit, is against the conclusion drawn from the Co/Ni ratio mentioned above, possibly meaning hydrothermal solutions of this style of gold mineralization originated from multiple sources. On the other hand, the S/Se ratios in Table 3 are below 9000–13000. Hu et al. (1990) published Se/Te and S/Se ratios in pyrites from the Xiaoyingpan deposit at 0.04–6.5 and 20,000–52,000, which are far from the criteria mentioned above, meaning that the replacement style of gold deposits has nothing to do with the magmatic solution, which is consistent with that of the Co/Ni ratio.

The As and Au contents in the pyrites tend to have a positive correlation with each other (Tables 2, 3, Fig. 6). Both previous researchers and the authors of this paper observed the presence of trace arsenopyrite, bismuthinite and stibnite under a microscope. Considering that the radii of both As^{3-} and $[S_2]^{2-}$ are very close to each other, it is very possible that As enters pyrite by replacing S as an isomorphous mixture. The As isomorphous mixture would make the unit cell parameters larger and chemical bonds

Table 2 Trace elements in pyrites from the representative gold mines

Gold mine	Series #	Pyrite style	Au	Ag	Cu	Pb	Zn	Co	Ni	Se	Te	As	Cr	Characteristic value			Data
			$\times 10^{-6}$											Au/Ag	Co/Ni	Co + Ni	Source
Xiaoyingpan	1	fg clot (?)[a]	210.00	194.0	4850	400	80	115	1000	< 0.1	40	–	–	1.08	0.12	1115	Hu et al. (1990)
	2	fg clot (?)	267.22	78.0	310	340	80	178	940	< 0.1	73	–	–	3.43	0.19	1118	
	3	cg Ds (?)	1.11	4.4	90	150	20	18	23	125.0	88	–	–	0.25	0.78	41	
	4	cg Ds (5)[b]	2320.00	380.0	550	–	2733	2980	1960	430.0	400	1320.0	460.0	6.11	1.52	4940	This paper
	5	fg clot (2)	5050.00	750.0	< 10	–	410	315	210	< 0.1	70	5550.0	2200.0	6.73	1.50	525	
Zhangquanzhuang	6	fg clot (?)	192.00	41.0	210	500	381	125	69	–	56	–	–	4.68	1.81	194	
	7	cg Ds (?)	5.22	111.1	40	1040	70	93	43	–	3	–	–	0.05	2.16	136	
	8	cg Ds (1)	–	1100.0	< 10	–	< 10	100	1000	400.0	280	500.0	–	–	0.10	1100	This paper
	9	fg clot (10)	3490.00	960.0	2370	–	1460	440	730	180.0	320	440.0	330.0	3.64	0.60	1170	
Jinjiazhuang	10	fg clot (?)	352.00	70.0	1200	250	70	188	116	–	–	–	22.0	5.03	1.62	304	Dong (1989)
	11	cg Ds (?)	60.00	15.0	115	13	50	53	25	–	–	–	17.0	4.00	2.12	78	
Shuijingtun	12	fg clot (?)	59.44	75.0	–	480	10	48	90	19.0	112	–	–	0.79	0.53	138	Hu et al. (1990)
	13	cg Ds (?)	2.23	12.5	1990	95	335	13	144	30.0	5	–	–	0.18	0.09	157	
Hougou	14	vnlt (?)	419.30	12.6	210	8300	140	90	120	0.1	< 1	6.4	–	33.17	0.75	210	Yin and Shi (1995)
	15	fg clot (?)	475.60	11.2	90	1700	30	80	150	< 0.1	< 1	7.9	–	42.46	0.53	230	
	16	fg mass (?)	493.50	9.4	110	1200	70	80	150	0.1	< 1	6.1	–	52.50	0.53	230	Hu et al. (1990)
	17	cg clot (?)	42.60	6.3	47	616	40	159	243	–	–	3.3	–	6.76	0.65	402	
Detection limit	0.01	0.1	10	10	10	10	1	0.1	1	0.1	0.1						
Au reference (STD OxP61)	14.82																
Au reference (STD ME1806)	3.31	362.0															
Reference—OREA210		1.2	183	13	130	37	111	7	–	3956	158						

Chemical analyses by the chemical lab, China University of Geosciences (Beijing)

fg = fine grained, cg = coarse grained, Ds = dissemination, vnlt = veinlet

[a]Number of sample unknown)

[b]Total number of sample

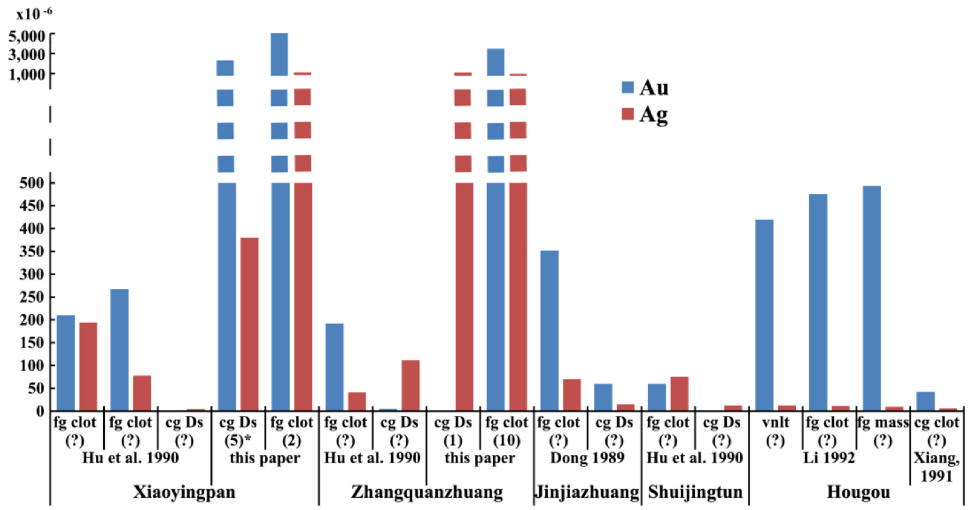

Fig. 2 Correlation between grain size of pyrite and its gold content

weaker. This would in turn make it easier for gold to enter the lattice defects of the pyrite crystals and result in gold-rich pyrites.

7 Unit cell parameters

The unit cell parameters of the pyrites are calculated and listed in Table 4. X-ray diffraction was performed at the lab of China University of Geosciences in Beijing. Compared to its standard parameter $\alpha = 5.417 \times 10^{-10}$ m (Jin and Li 1985; Chen 1987), the following can be seen:

Each α_0 of the three coarse-grained pyrites from the Xiaoyingpan gold deposit is smaller than the standard α_0, and their average value (5.415×10^{-10} m) is smaller than that of the six fine-grained pyrites (5.4189×10^{-10} m) from the same deposit. This should be due to more As, Co, Ni, Au, and Ag entering fine-grained pyrite than coarse-grained pyrite.

Both the average α_0 (5.41895×10^{-10} m) and v_0 (159.1275×10^{-30} m^3) of pyrites from Zhangquanzhuang deposit are bigger than those (respectively $\alpha_0 = 5.41760 \times 10^{-10}$ m and $v_0 = 159.0080 \times 10^{-30}$ m^3) of pyrite from Xiaoyingpan deposit, possibly meaning that both the ore type (poor and rich sulfide ores) and metallogenic condition of the two styles of deposits are different from each other to some degree.

The v_0 of pyrites from both representative deposits has a generally positive correlation trend with the gold content of pyrite samples (Fig. 7).

The average α_0 (5.41989×10^{-10} m) and v_0 (159.2103×10^{-30} m^3) of the pentagonal dodecahedral pyrites are greater than those of the cubic pyrites from the Zhangquanzhuang deposit, which are $\alpha_0 = 5.41844 \times 10^{-10}$ m and $v_0 = 159.1091 \times 10^{-30}$ m^3, respectively. According to Chen (1987), this is because it is easier for pentagonal dodecahedron pyrite to accept As than for cubic pyrite, and pentagonal dodecahedron pyrite forms at a higher As concentration than cubic pyrite.

It is worth saying that the X-ray diffraction intensity of pyrite rich in gold is lower than that of pyrite poor in gold from the Zhangquanzhuang deposit. In general, as gold content increases in pyrite, the total sum intensity ΣI decreases. Pyrites rich in gold usually contain higher Au, Ag, Co, Ni, As, Se, and Te contents, which result in lattice plane net defects when these trace elements enter pyrite, and the defects in turn result in lattice defect scattering when X-rays irradiate the plane net with defects and decrease the X-ray intensity.

8 Pyroelectricity characteristics

The pyroelectricity characteristics of the pyrites are listed in Table 5 and further summarized in Table 6 based on Tables 2, 3 and 5. The pyroelectricity test was performed in a lab at the China University of Geosciences in Beijing.

Based on Tables 5 and 6, it can be preliminarily concluded that.

- The pyroelectricity coefficient a has a negative correlation trend with the values of (Co + Ni + Se + Te)–As and (Co + Ni + Se + Te)/As in pyrites, except for the # ZE790-19–01-2 sample in Table 6. Namely, when values of (Co + Ni + Se + Te)–As and (Co + Ni + Se + Te)/As increase, a decrease, and the conduction

Table 3 Electron microprobe analysis results of pyrites from the representative gold mines

Gold mine	Series #	Sample #	Style	Assay results (wt%)													Characteristic value					
				S	Fe	Co	Ni	Cu	Zn	Cr	As	Sb	Se	Te	Au	Ag	S/Fe[(a)]	Co/Ni	Co + Ni	Au/Ag	Se/Te	S/Se
Xiaoyingpan	1	PD1-04	cg cube	53.34	44.49	0.54	0.73	0.00	0.32	0.09	0.23	–	0.09	0.00	0.00	0.08	1.16	0.74	1.27	0.00	–	592.67
	2	HS1-04	cg cube	53.67	45.23	0.00	0.03	0.20	0.08	0.05	0.00	–	0.00	0.04	1.16	0.00	1.18	0.00	0.03	–	0.00	–
	3	HS1-05	cg cube	54.03	44.48	0.73	0.00	0.02	0.42	0.00	0.00	–	0.04	0.00	0.00	0.00	1.19	–	0.73	–	–	1350.75
	4	HS1-05	fg cube	52.63	44.84	0.56	0.22	0.00	0.41	0.22	0.11	–	0.00	0.07	0.00	0.03	1.15	2.55	0.78	0.00	0.00	–
	5	XS5-04	cg cube	53.03	46.35	0.00	0.22	–	–	–	0.00	0.00	–	–	0.00	0.11	–	0.00	0.22	0.00	–	–
	6	XS5-04	fg cube	53.11	45.75	0.07	0.20	–	–	–	1.00	0.14	–	–	1.01	0.12	–	0.35	0.27	8.42	–	–
	7	XD-012	cg cube	53.03	46.04	0.16	0.00	–	–	–	0.43	0.13	–	–	0.00	0.00	–	–	0.16	–	–	–
Zhangquanzhuang	8	ZE790-1–01	fg cube	52.36	47.71	0.00	0.07	0.04	0.12	0.07	0.10	0.00	0.00	0.00	0.04	0.02	1.09	0.00	0.07	2.00	–	–
	9	ZE790-1–01	fg PD	52.32	46.49	0.00	0.00	0.00	0.09	0.00	0.07	0.04	0.06	0.11	0.00	0.09	1.13	–	0.00	0.00	0.55	872.00
	10	ZE790-15–01	cg cube	54.00	46.36	0.01	0.10	0.00	0.00	0.00	0.05	0.01	0.04	0.03	0.00	0.11	1.16	0.10	0.11	0.00	1.43	1350.00
	11	ZE790-15–01	fg PD	53.45	46.49	0.00	0.00	0.00	0.44	0.03	0.12	0.00	0.07	0.00	0.00	0.00	1.15	–	0.00	–	–	763.57
	12	ZE790-19–01	fg cube	53.63	46.09	0.00	0.00	0.00	0.32	0.03	0.00	0.00	0.03	0.03	0.55	0.16	1.16	–	0.00	3.44	1.00	1787.67
	13	ZE790-19–01	mg PD	53.99	46.99	0.00	0.00	0.01	0.00	0.04	0.00	0.01	0.00	0.00	0.00	0.08	1.15	–	0.00	0.00	–	–
	14	ZE790-19–01	fg PD	53.13	46.15	0.00	0.00	0.00	0.26	0.06	0.02	0.00	0.00	0.00	0.00	0.07	1.00	–	0.00	0.00	–	–
	15	ZE830-2–01	fg cube	51.08	44.22	0.30	0.30	1.89	0.00	0.00	0.00	0.32	0.00	0.00	1.07	0.09	1.15	1.00	0.60	11.89	–	–
	16	ZE830-01	fg cube	53.42	45.72	0.00	0.13	0.15	0.00	0.00	0.00	0.00	0.00	0.00	1.17	0.00	1.14	0.00	0.13	–	–	–
	17	ZE830-06	fg cube	52.55	44.81	0.02	0.01	0.00	0.23	0.04	0.00	0.02	0.00	0.18	0.25	0.31	1.17	2.00	0.03	0.81	0.00	–
	18	ZE870-8–05	fg cube	53.66	45.51	0.12	0.22	0.28	0.00	0.06	0.13	0.00	0.02	0.00	0.41	0.14	1.17	0.55	0.34	2.93	–	2683.00

Analyses by the electron microprobe lab, China University of Geosciences (Beijing)

cg, Coarse grained; fg, fine grained; PD, Pentagonal dodecahedron; mg, Medium grained

[(a)]Fe = Fe + Co + Ni + Cr

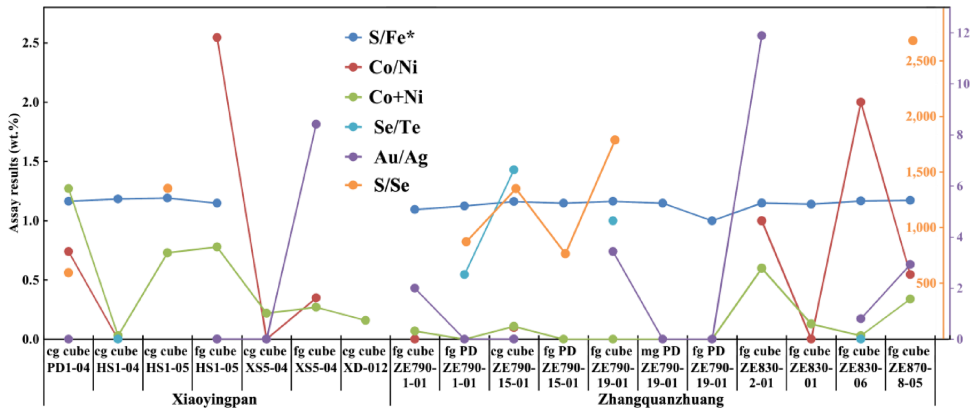

Fig. 3 S/Fe ratio comparison of pyrites from both Xiaoyingpan and Zhangquanzhuang gold deposits

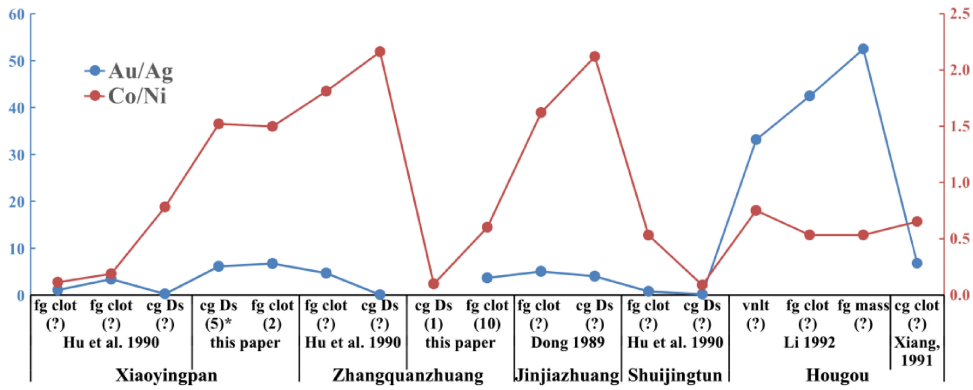

Fig. 4 Au/Ag and Co/Ni ratio comparisons in pyrite from both the Xiaoyingpan and Zhangquanzhuang deposits

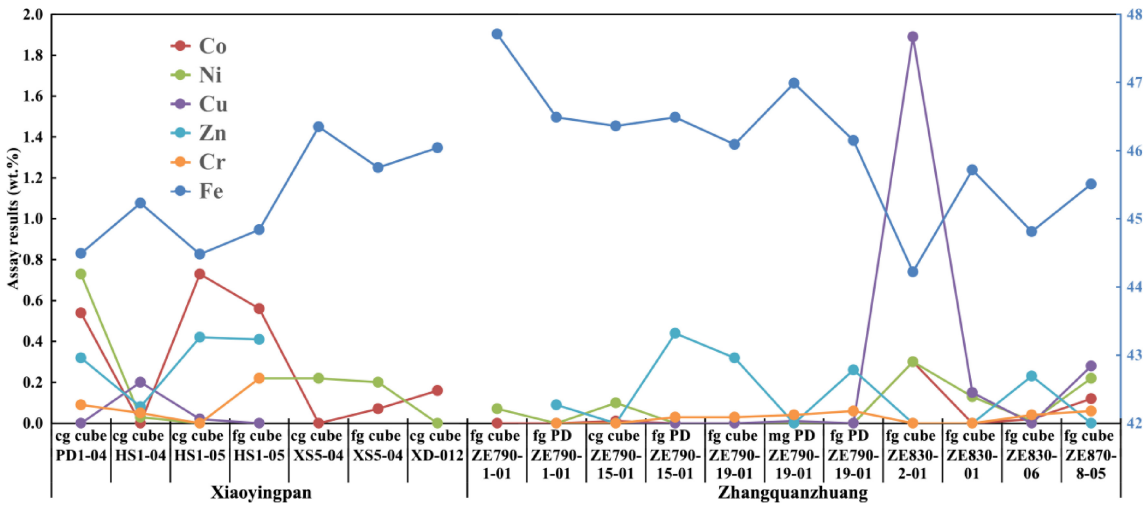

Fig. 5 Spider diagram of various elements in pyrites from both the Xiaoyingpan and Zhangquanzhuang deposits

type contains more N type than P-type, and finally becomes N type completely (Fig. 8).

- The pyroelectricity of the pyrites does not have any regular relationship with either its crystal form or gold content (Fig. 9).
- The pyrite pyroelectricity of the Xiaoyingpan deposit is N-type, indicating that it formed under low sulfur fugacity, while that of the Zhangquanzhuang deposit is a P-N mixed type, indicating that it formed under high sulfur fugacity (Fig. 10). Meanwhile, pyrite

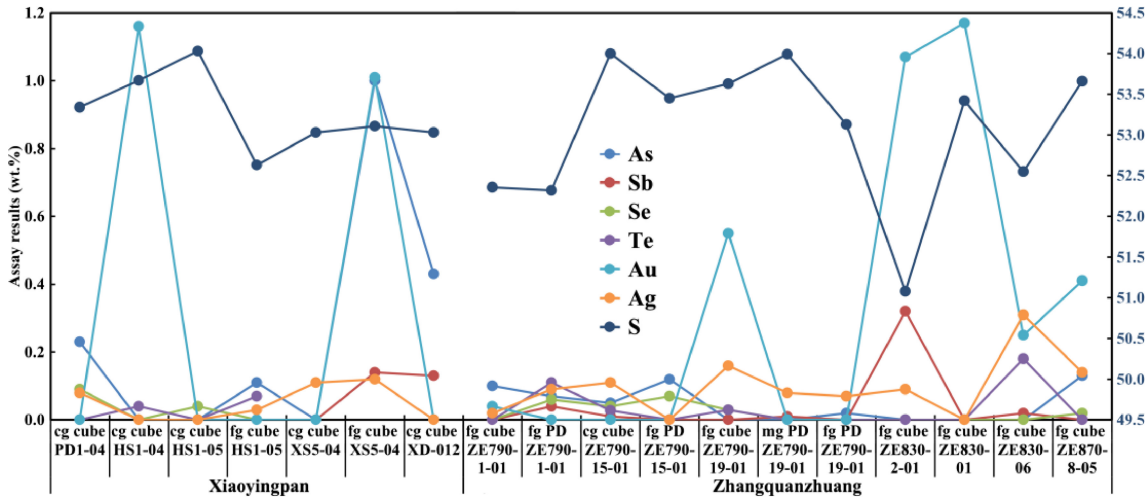

Fig. 6 Spider diagram of various elements in pyrites from both the Xiaoyingpan and Zhangquanzhuang deposits

pyroelectricity shows that the formation of Xiaoyingpan has something to do with metamorphism, while that of Zhangquanzhuang has to do with hydrothermal superposition. Comprehensively considering the ore control structures, host rocks, and other geological controls of the two styles of gold deposits, it is probable that the current mining level of the former mine is the root part of the whole mineralized bodies, while the latter is the middle part of the total ore bodies. As a result, the ore-hunting target for the Xiaoyingpan mine is not at depth but instead along strike around the present mining site, while that for the Zhangquanzhuang mine is both at depth and along strike around the current mining site.

- On the pyroelectricity-temperature diagram (Fig. 11), pyrite from Xiaoyingpan is mainly distributed between 200 and 270 °C, while that from Zhangquanzhuang is distributed within 90–118 °C and 274–386 °C, showing a multistage formation process.

9 Electron paramagnetic resonance spectrum

The EPR test was carried out on pyrites from both Xiaoyingpan and Zhangquanzhuang mines to confirm whether there is any lattice gold available in the area. The results are shown in Fig. 12 and listed in Table 7. In Table 7, $g = h^*\gamma/\beta^*H$, h is the Planck constant, where γ is the resonance frequency, β is the Bohr magneton (9.27×10^{-21} erg/Gauss), and H is the add-on magnetic field intensity; the g factor of free electrons used here is $g_e = 2.0023$.

The linear type in Table 7 was determined by the use of the differential slope method. The absorption peak of the G type is narrow and decays fast, while that of the L type is wide, gentle, and decays slowly.

According to Fig. 12 and Table 7, auriferous pyrite has more absorption peaks than gold-free pyrite. In addition to a wide-gentle L and/or G-L mixture absorption peak (I), the former also has one or two narrow G absorption peaks (II & III), while the latter has only one wide-gentle L absorption peak (I). All gold-bearing pyrites have a narrow # II absorption peak, of which both $ZY/\Delta Hpp$ and I_N are larger than those of the other two peaks (Fig. 13). The calculated g factor of this peak ranges between 1.987351 and 2.00425, of which most is concentrated at 2.0023, namely, around $g_e = 2.0023$. The existence of the peak has a close relationship with the gold present in pyrites.

The affiliation attribute and mechanism of the EPR bands/lines of the pyrites are discussed as follows.

9.1 Absorption peaks I and III

According to Table 7, the g factors of peaks I and III are greater than $g_e = 2.0023$ (Fig. 14). The g factor determines the position of the EPR bands/lines and only has something to do with the physical properties of the sample. Free electrons here refer to electrons with only spin angular momentum but without orbital angular momentum. General transition metal ions have both spin and orbital angular

Table 4 Unit cell parameters of pyrites from the representative gold mines

Gold mine	Series #	Sample #	Style	Unit cell parameter					Au
				α_0 ($\times 10^{-10}$m)	v_0 ($\times 10^{-30}$m^3)	Max. d value [(111) planar net]	d value when I = 100 [(311) planar net]	ΣI	$\times 10^{-6}$
Xiaoyingpan	1	PD1-04	cg cube	5.41491	158.7715	3.125	2.706	443	–
	2	HS1-01	fg cube	5.41969	159.1926	3.132	2.712	401	(Au diffracted ray)
	3	HS1-04	fg cube	5.41781	159.0269	3.132	2.709	364	33.71 (Au diffracted ray)
	4	HS1-04	cg cube	5.41609	158.8757	3.125	1.633	400	–
	5	HS1-05	fg cube	5.41895	159.1276	3.132	1.634	459	–
	6	HS2-06	fg cube	5.42308	159.4915	3.136	1.635	466	–
	7	XS5-01	cg cube	5.41414	158.7044	3.123	2.706	415	–
	8	XS5-01	fg cube	5.41452	158.7376	3.123	1.632	495	15.11
	9	XD-012	fg cube	5.41922	159.1511	3.132	1.634	465	–
	Average			5.41760	159.0088	3.129			
Zhangquanzhuang	10	ZE790-12–02	fg cube	5.42215	159.4092	3.134	2.714	460	–
	11	ZE790-12–04	fg cube	5.42106	159.3138	3.134	1.635	482	–
	12	ZE790-13–02	fg cube	5.41653	158.9141	3.127	1.633	422	5.57
	13	ZE790-13–02	fg PD	5.41963	159.1879	3.132	2.711	398	8.65
	14	ZE790-15–01	fg cube	5.41463	158.7477	3.125	2.709	371	–
	15	ZE790-17–02	fg cube	5.42292	159.4779	3.136	1.635	439	–
	16	ZE790-19–01	fg cube	5.41317	158.6186	3.121	2.703	391	–
	17	ZE790-19–01	fg PD	5.42014	159.2327	3.132	1.634	417	5.43
	18	ZE790-19–02	fg cube	5.41759	159.0077	3.127	1.633	404	–
	19	ZW870-10–07	fg cube	5.42096	159.3046	3.134	1.635	408	29.25
	20	cyp-01	fg cube	5.41963	159.1879	3.132	2.711	335	–
	Average			5.41895	159.1275	3.130			

cg, Coarse grained; fg, Fine grained; PD, Pentagonal dodecahedron; ΣI, $I_1 + I_2 + \cdots I_{11}$

Analysis by the X-ray Diffraction lab, China University of Geosciences (Beijing)

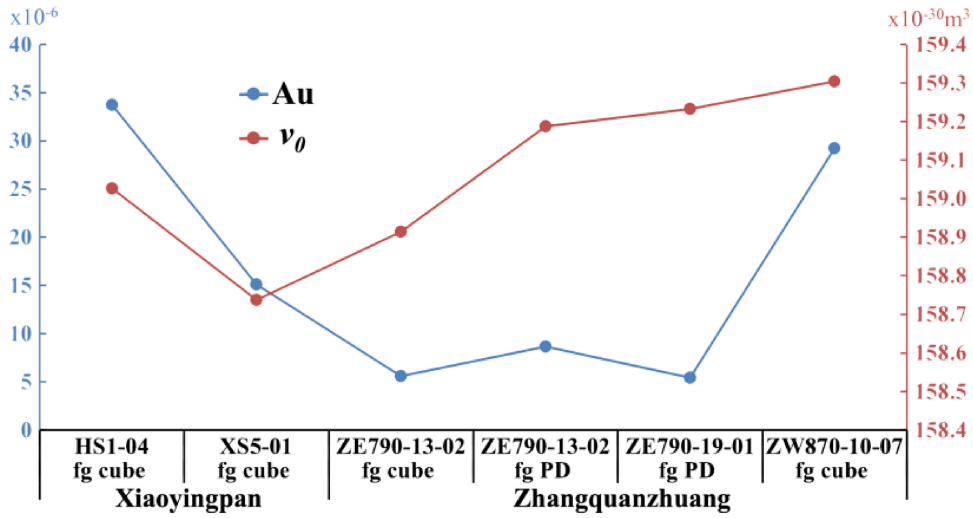

Fig. 7 The v_0 of pyrites has a generally positive correlation trend with the gold content of the samples

momenta. As a result, their g factors are far from g_{e-} = 2.0023. According to Chen (1987), when the d shell electron of the transition metal ions is below half full, $g < g_e$; when the d shell electron of transition metal ions is above half full, $g > g_e$; additionally, when the d shell electron of transition metal ions is just half full, $g \approx g_e$. As a result, the $g > g_e$ absorption peaks I and III in Figs. 12 and 14 results from transition metal ions with d shell electrons above half full.

The best material abundance range for EPR testing was (10–1,000) × 10^{-6}. Ions that could produce spectra at room temperature include Cr^{3+}, Mn^{2+}, Fe^{2+}, Ni^{2+}, and Cu^{2+} (Jin and Li 1985; Chen 1987). As discussed above, it is common for pyrite in the area to contain Cr^{3+}, Ni^{2+}, and Cu^{2+} (Tables 2, 3). The d shell electron of Cr^{3+} is below half full and its $g < g_e$, which conflicts with the EPR result. Thus, Cr^{3+} has nothing to do with absorption peaks I & III. Therefore, absorption peaks I & III could only be produced by the resonance absorptions of Ni^{2+} and/or Cu^{2+}.

9.2 Absorption peak II

When the symmetry described by the crystal space group is destroyed, crystal structure defects occur. These defects then destroy the original electric neutrality locally and form a variety of "defect centers" in the crystal. For example, when the defect vacancy of an anion or cation is replaced by another cation with a more positive charge, the crystal structure position shows a positive charge owing to the lack of a negative charge and becomes an electron trap. This position would become an electron center when capturing one or more electrons. If the defect vacancy of a cation and/or some cations is replaced by another cation with a less positive charge, this crystal structure position would show a negative charge owing to a lack of positive charge and become a positive electron trap; under certain conditions, for instance, under irradiation, an anion next to this position would lose surplus electrons and produce a hole center.

The study targets of EPR are these electron–hole centers available in the crystal structure. The EPR band/line produced by these electron–hole centers is extremely narrow and $g \approx g_e$ and has only one fine line. It is clear that the absorption peak II in Fig. 12 results from the electron–hole centers in the pyrites. Since the comparative sample in Fig. 12 is gold-free and does not have an absorption peak II, it can now be concluded that absorption peak II results from gold entering the pyrite structure.

Now, it is time to determine in which chemical form, Au^0, Au^+, or Au^{3+}, gold enters the pyrite lattice.

9.2.1 Supposing in the form of Au^0 and/or Au^{3+}

The outer shell electron configuration of Au is $5d^{10}6s^1$, meaning that both Au^0 and Au^{3+} have unpaired electrons on their outer electron orbitals. Considering their spin magnetic moment I = 3/2, either of them should produce an obvious superfine structure on the EPR image if available in pyrite, but the fact is that this kind of structure does not appear in Fig. 12. As a result, it can be concluded that gold in pyrite is neither in the form of Au^0 nor Au^{3+}.

Table 5 Pyroelectricity of pyrites from the representative gold mines

Gold mine	Series #	Sample #	Style	Pyroelectricity $a(\mu V/°C)$				Au
				TVG[(a)]	Average	CT[(b)]	N%[(c)]	$\times 10^{-6}$
Xiaoyingpan	1	PD1-04–01	cg cube	(− 180.714 to − 502.857)	− 300.136	N	100	
	2	PD1-04–02	fg cube	(− 133.571 to − 461.429)	− 290.000	N	100	
	3	HS1-04–01	cg cube	(− 186.429 to − 387.857)	− 287.680	N	100	
	4	HS1-04–02	mcg cube	(− 166.428 to − 391.428)	− 299.860	N	100	
	5	HS1-04–03	fg cube	(− 207.857 to − 379.286)	− 299.960	N	100	33.71
	6	HS1-05–01	mcg cube	(− 236.428 to − 429.286)	− 313.360	N	100	
	7	HS1-05–02	fg cube	(− 237.143 to − 434.286)	− 338.680	N	100	
	8	HS2-06	fg cube	(− 146.429 to − 348.571)	− 239.200	N	100	
	9	XS5-01–1	cg cube	(− 205.714 to − 502.857)	− 323.420	N	100	
	10	XS5-01–2	fg cube	(− 127.143 to − 409.286)	− 268.540	N	100	15.11
	11	XS5-10	Fe stained cube	(− 150.000 to − 337.857)	− 223.960	N	100	
	12	XD-012	Subhydron, anhydron	(− 237.857 to − 530.000)	− 361.820	N	100	
	Average			(− 236.428 to − 429.286)	− 295.551	N	100	
Zhangquanzhuang	13	ZE790-12–2-1	mcg cube	(− 320.714 to + 312.857)	15.860	P–N	55	
	14	ZE790-12–2-2	fg cube	(− 315.000 to + 382.857)	60.857	N–P	40	
	15	ZE790-12–2-3	fg PD	(− 109.286 to + 386.429)	187.180	N–P	15	
	16	ZE790-12–4	Cube + a few PD	(− 210.000 to + 280.000)	35.460	N–P	35	
	17	ZE790-13–2-1	fg cube	(− 349.286 to + 345.000)	28.460	N–P	45	5.57
	18	ZE790-13–2-2	fg PD	(− 209.286 to + 318.571)	− 43.607	P–N	60	8.65
	19	ZE790-15–1	fg cube	(− 438.571 to + 032.143)	− 165.250	P–N	90	
	20	ZE790-17–2	Cube + PD	(− 290.714 to + 277.143)	− 129.390	P–N	70	
	21	ZE790-18–1	Cube + PD	(− 232.143 to − 114.287)	− 175.960	N	100	
	22	ZE790-19–1-1	cg cube	(− 455.714 to + 489.286)	− 30.210	P–N	55	
	23	ZE790-19–1-2	fg cube	(− 321.428 to + 330.000)	− 62.350	P–N	75	
	24	ZE790-19–1-3	fg PD	(− 340.000 to + 097.143)	− 194.360	P–N	90	5.43
	25	ZE790-19–4	fg PD	(− 365.000 to − 090.714)	− 212.190	N	100	
	26	ZW830-01	fg cube	(− 288.571 to + 080.000)	− 156.610	P–N	90	
	27	ZW830-02	fg cube	(− 242.143 to + 073.571)	− 112.600	P–N	84	
	28	ZW870-10–07	fg subhydron	(− 284.286 to + 215.714)	− 117.120	P–N	80	29.25
	29	CYP-01	Subhydron, anhydron	(− 275.571 to + 044.286)	− 179.560	P–N	89	
	Average			− 73.605				
Excitation temperature		140 °C						

Each single sample was composed of 20 grains of pyrite mineral which were chosen randomly. Test by the lab of geology of mineral deposits sector, China University of Geosciences (Beijing)

cg, coarse grained, fg, fine grained, mcg, medium to coarse grained, PD, pentagonal dodecahedron

[(a)]Thermoelectric voltage range

[(b)]Conduction type

[(c)]Percentage of N type

9.2.2 Supposing in the form of Au^+

This should be the only possibility after eliminating Au^0 and Au^{3+}.

Au^+ ($5d^{10}$), as a nonparamagnetic ion, would break the charge balance of the whole system and produce charge compensation after replacing Fe^{2+} as an isomorph. Since the majority of valence bonds in the pyrite structure are covalent, this would produce hole centers on the S–S bond, namely, the electron–hole centers. In other words, the FeS_2 system obtains an "electron" that produces the EPR resonance absorption information, which is equivalently a free radical with only a spin magnetic moment and without an orbit magnetic moment, and its $g \approx g_e$. This aligns

Table 6 Relationship between pyroelectricity and trace elements in pyrites from representative gold mines

Series #	Sample #	Style	Co + Ni	Se + Te	As	(Co + Ni + Se + Te)–As	(Co + Ni + Se + Te)/As	Averaged pyroelectricity *a*(μV/°C)	CT[(a)]	N%[(b)]
			% of atomic mass							
1	PD1-04	cg cube	0.870	0.040	0.120	0.790	7.580	− 300.126	N	100
2	HS1-04	cg cube	0.430	0.010	0.000	0.440	–	− 287.680	N	100
3	HS1-05–01	mcg cube	0.540	0.020	0.000	0.560	–	− 313.360	N	100
4	HS1-05–02	fg cube	0.540	0.020	0.060	0.560	9.330	− 338.680	N	100
Average		0.595	0.023				− 309.962	N	100	
5	ZE790-15–1	fg cube	0.070	0.100	0.030	0.140	5.670	− 165.250	P–N	90
6	ZE790-19–01-1	fg cube	0.000	0.030	0.000	0.030	–	− 62.350	P–N	55
7	ZE790-19–01-2	fg PD	0.000	0.000	0.010	− 0.010	0.000	− 194.360	P–N	75
8	ZW830-01	fg cube	0.090	0.000	0.000	0.090	–	− 156.610	P–N	90
Average			0.040	0.010						

PD, Pentagonal dodecahedron; cg, Coarse grained, mcg, Medium to coarse grained, fg, Fine grained

[(a)]Conduction type

[(b)]Percentage of N type

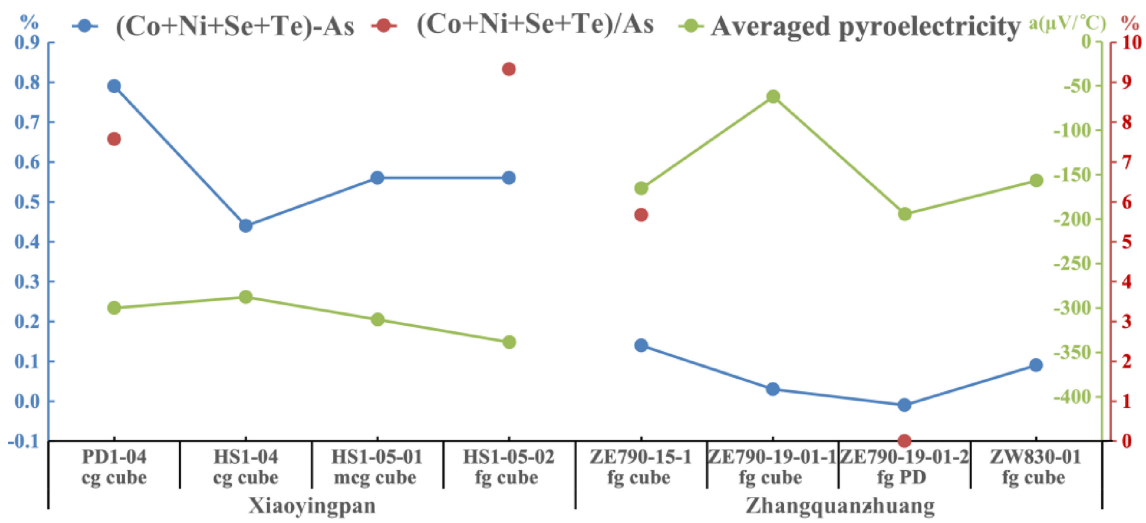

Fig. 8 Relationship between pyroelectricity coefficient *a* and [(Co + Ni + Se + Te)-As] as well as (Co + Ni + Se + Te)/As of pyrites

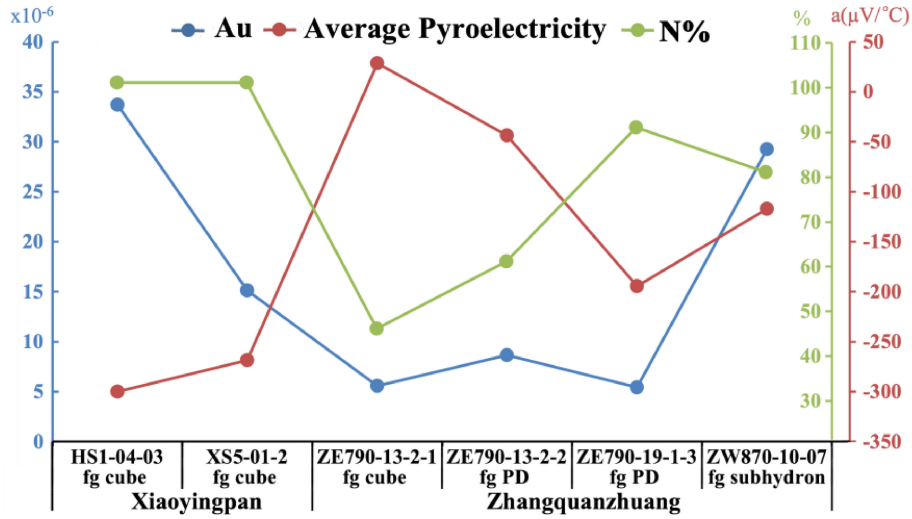

Fig. 9 Diagram of the pyroelectricity *a* of pyrite—gold content in the samples

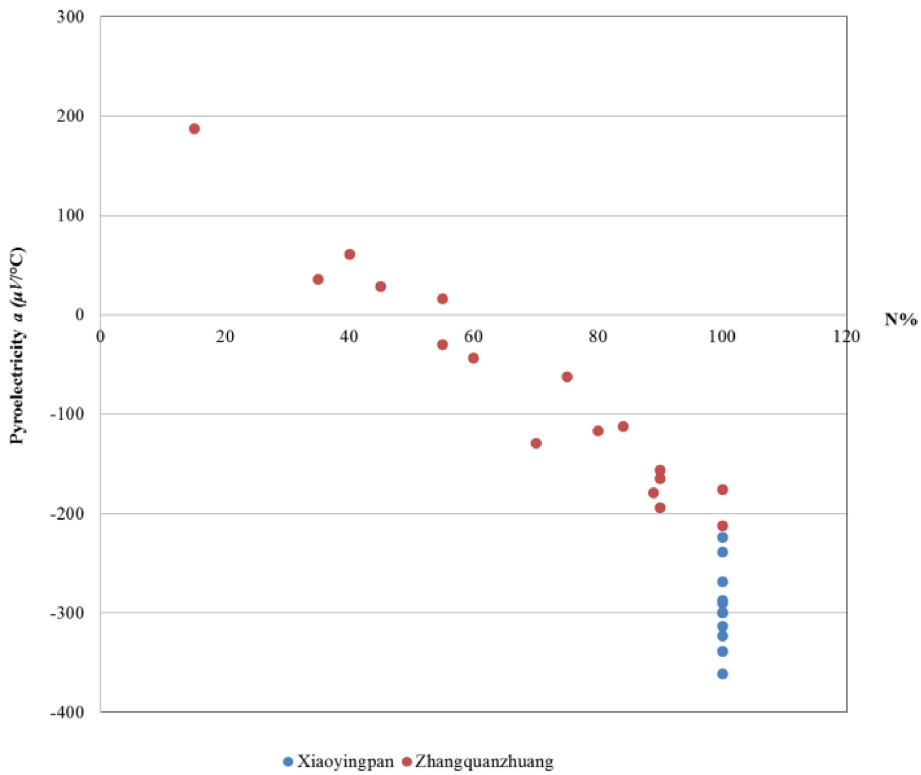

Fig. 10 Contrast of pyroelectricity *a* of the pyrites from both Xiaoyingpan and Zhangquanzhuang gold mines

completely with the characteristics of absorption peak II in this paper. With increasing Au^{+} entering the pyrite lattice, an increasing number of electron–hole centers are produced, and the density of electron–hole centers increases. As a result, the signals of the EPR absorption peak are enhanced accordingly, and the intensity of absorption peak II can be used to determine the gold content in pyrite.

Based on the discussions above, it can be preliminarily concluded that:

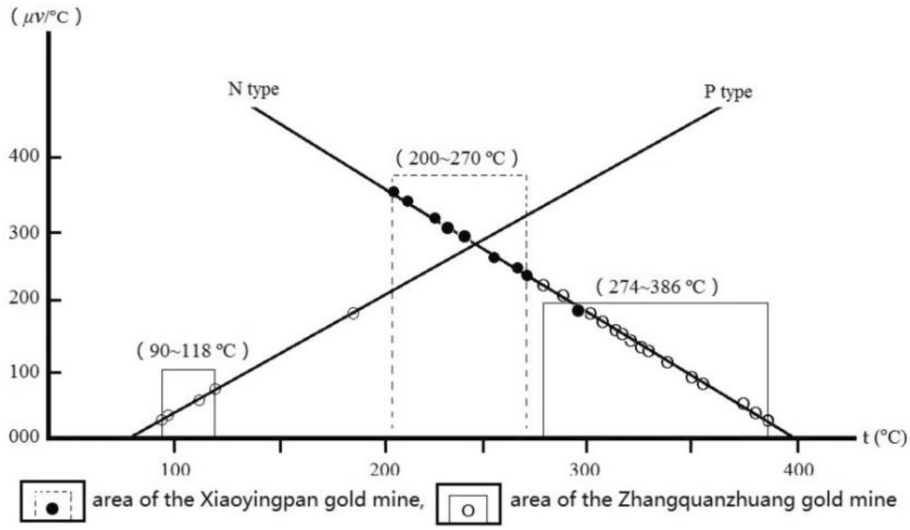

Fig. 11 Pyroelectricity-temperature diagram of pyrites from the study area

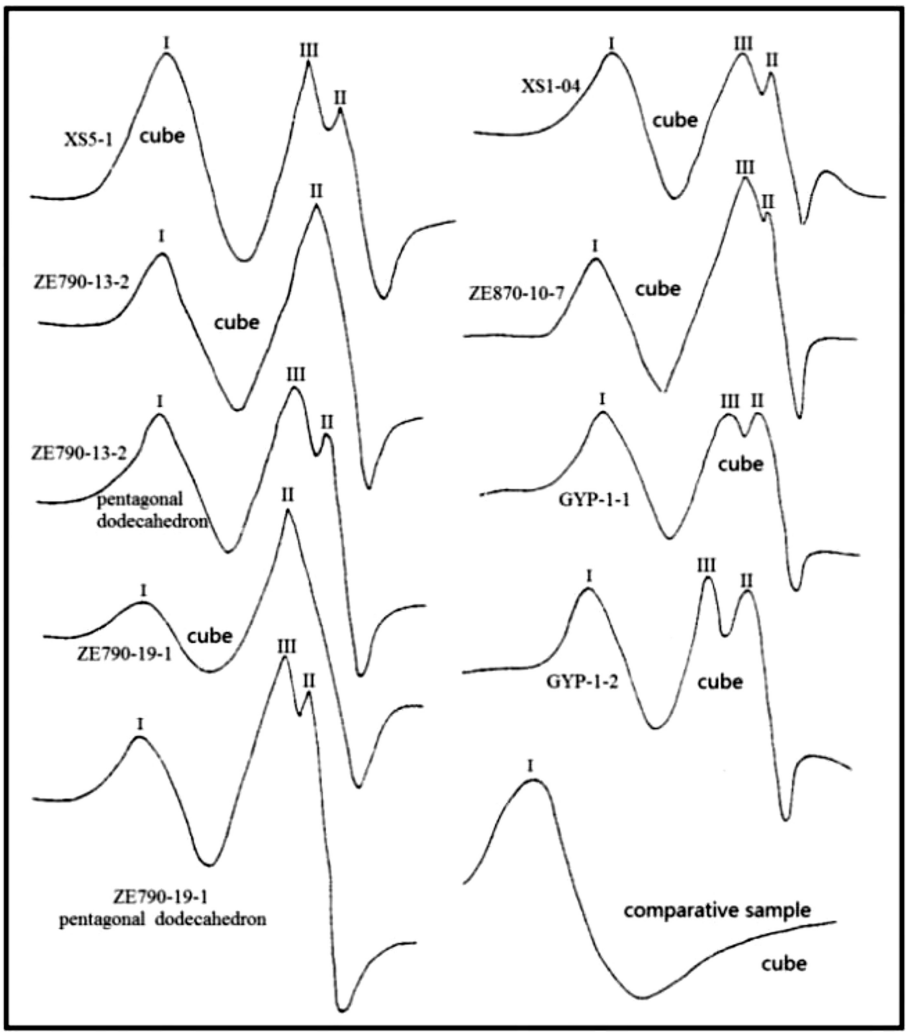

Fig. 12 EPR spectra of pyrites from the representative gold deposits when T = 295 K (Lab: EPR lab of the Department of Physics, Peking University, China)

Table 7 Calculated EPR parameters of pyrites from the representative gold mines

Mine	Series #	Sample #	Style	Absorption peak		EPR parameter						Au	Linear
				Number	Labelling	*ZY* (PA [(a)]) cm	*ΔHpp*(PW[(b)]) G	*ZY/ΔHpp* × 10^{-3}	Intensity *I*	I_N (NI[(c)]) × 10^{-5}	g-factor value	× 10^{-6}	Type
Zhangquanzhuang	1	ZE790-13–2	fg cube	2	I	9.30	507.5	18.32	2,395,273	1.16	2.8688	5.57	G–L
					II	15.50	360.0	43.06	2,008,800	1.94	2.0024		G
			fg PD	3	I	8.54	475.0	17.98	1,926,837	2.14	2.8656	8.65	G–L
					II	15.27	337.5	45.24	1,739,348	3.82	2.0043		G
					III	3.17	100.0	31.70	31,700	0.80	2.1760		G
	2	ZE790-19–1	fg cube	2	I	4.50	490.0	9.18	1,080,450	1.12	2.9128	–	L
					II	18.20	512.5	35.51	4,780,343	4.55	2.0024		G
			fg PD	3	I	9.47	540.0	17.54	2,761,452	1.18	2.8811	5.43	G–L
					II	24.14	390.0	91.90	3,671,694	3.02	2.0019		G
					III	3.04	45.0	67.56	6156	0.38	2.1698		G
	3	ZW870-10–7	fg cube	3	I	8.15	482.8	16.89	1,897,370	1.02	2.8777	29.25	G–L
					II	12.62	232.5	54.28	682,189	1.58	1.9874		G
					III	2.71	87.5	3.10	20,748	0.34	2.0978		G
	4	cyp-1–1	fg cube	3	I	7.51	465.0	16.15	1,623,849	0.94	2.8864	–	G
					II	10.84	290.0	37.39	911,644	1.36	2.0043		G
					III	2.23	75.0	29.73	12,544	0.28	2.1897		G
	5	cyp-1–2	fg cube	3	I	8.45	450.0	18.78	1,711,125	1.05	2.8810	–	G
					II	13.55	300.0	45.17	1,219,500	1.69	2.0018		G
					III	3.54	85.0	41.65	25,576	0.44	2.2321		G
Xiaoyingpan	6	HS1-04	fg cube	3	I	8.48	480.0	17.67	1,953,792	1.06	2.8709	33.71	G–L
					II	9.14	265.0	34.49	641,856	1.14	2.0020		G
					III	2.32	125.0	18.56	36,250	0.29	2.1487		G
	7	XS5-1	fg cube	3	I	11.74	65.5	17.99	4,998,378	1.47	2.7454	15.11	G–L
					II	10.67	335.0	31.85	1,197,440	1.33	2.0024		G
					III	4.56	120.0	38.00	65,664	0.57	2.2430		G
Woxi, Hunan	8	V3W-23–13	n/a	2	I	3.20	550.0	5.82	485,000	–	2.0004	254.4	L
					II	1.60	18.8	85.33	281	–	2.0019		G
	9	V3E-24–14	n/a	2	I	1.20	525.0	2.29	165,000	–	2.0361	31.40	L
					II	0.70	12.5	56.00	54.6875	–	2.0021		G

Table 7 continued

Mine	Series #	Sample #	Style	Absorption peak		EPR parameter						Au	Linear
				Number	Labelling	ZY (PA [(a)]) cm	ΔHpp(PW[(b)]) G	$ZY/\Delta Hpp$ $\times 10^{-3}$	Intensity I	I_N (NI[(c)]) $\times 10^{-5}$	g-factor value	$\times 10^{-6}$	Type
Blank	10	CP****	cg cube	1	I	20.80	1450.0	14.34	43,732,000	65	4.6529	0.00	L

$I,ZY^*\Delta Hpp^2$, I_N , ZY/n (n is the amplication factor), L: Lorentz linear type, G: Gauss linear type, G-L: mixed or transitional linear type; pyrite samples. V3W-23–13 and V3E-24–14 are from the Woxi gold deposit in Hunan Province, China and provided by Wang Xueming and Mengxiong Chen. $g = h\gamma/\beta H = 0.714487\gamma$ (GHz)/H (kG), h is the Planck constant, γ is the resonance frequency, β is the Bohr magneton (9.27 × 10–21 erg/gauss), and H is the add-on magnetic field intensity; g factor of free electrons used here is g_e = 2.0023. Lab conditions: T = 295 K, microwave frequency 9.744–9.779 GHz, microwave power 10mW, magnification times 5 × 10^5, scanning scope ± 2500G, scanning time 500 s, rated magnetic field 5000G, home position 2500G, modulation amplitude: 3.2G, equipment: BRUKER ER200D-SRC

fg, Fine grained; PD, Pentagonal dodecahedron; cg, Coarse grained

(a)Peak amplitude

(b)Peak width

(c)Normalized intensity

- In contrast to previous research conclusions, lattice gold does exist in pyrites from gold deposits in the study area. Au, in the form of Au^+, entering pyrite as an isomorph and producing electron–hole centers, makes the centers produce spin resonance absorption and results in EPR absorption peak II.
- Auriferous pyrite has more EPR absorption peaks than pyrite without gold. The latter only has one gentle and wide L-type absorption peak, while the former has one or two narrower G-type absorption peak(s), in addition to the similar/same L-type peak as the latter.
- The I and III absorption peaks of the pyrites possibly result from the existence of Ni^{2+} and/or Cu^{2+}.
- The intensity of auriferous pyrite absorption peak II has certain direct positive correlations with the gold content in pyrite.

10 Infrared spectroscopic analysis

To confirm the infrared spectroscopic characteristics of the auriferous pyrites, infrared spectroscopic analysis (ISA) was conducted on powders of the pyrite samples in different forms and various grain sizes from the representative gold deposits in the study area. The results are shown in Fig. 15 and Table 8.

If the infrared spectrum absorption peaks are numbered γ_1, γ_2, γ_3, γ_4 and γ_5 from high to low wavenumbers, γ_1, and γ_2 would be the expansion vibration absorption spectroscopic bands of Fe-S bonds in pyrite, γ_3 would be the bending vibration absorption spectroscopic band, and $\gamma 4$ and γ_5 would be the vibration and rotation absorption spectroscopic bands of the crystal framework in pyrite. Due to the weak absorption and multiple interference signals at the bands, γ_4 and γ_5 do not always appear. It can be seen from both Fig. 15 and Table 8 that:

- The γ_1, γ_2, γ_3, and γ_5 absorption peaks appear on all ISAs of the pyrites, of which γ_1, γ_2, and γ_3 are the strongest, namely, the typical absorption peaks. Some of the pyrite samples produce weak absorption peaks at a wavenumber of approximately 270 cm^{-1}.
- The intensity, highest base intensity, wavenumbers, and intensity ratios of the corresponding absorption peaks of different pyrite samples differ from each other (Figs. 16, 17). These differences are embodied in the differences and changes of the calculated absorbance D (= $\log T_0/T$, T_0 is the light energy transmitted through a reference blank sample, while T is the light energy transmitted through the pyrite sample) and the relative absorbance values in Table 8 and Figs. 16 and 17.
- By comparing the infrared spectra, calculated parameters, and gold content of the pyrite samples, it can be

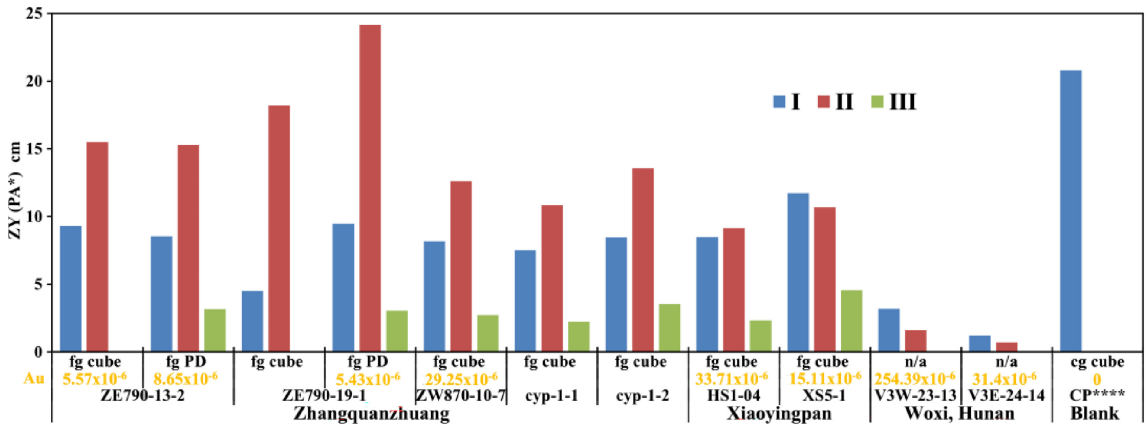

Fig. 13 Auriferous pyrite has more EPR absorption peaks than gold-free pyrite

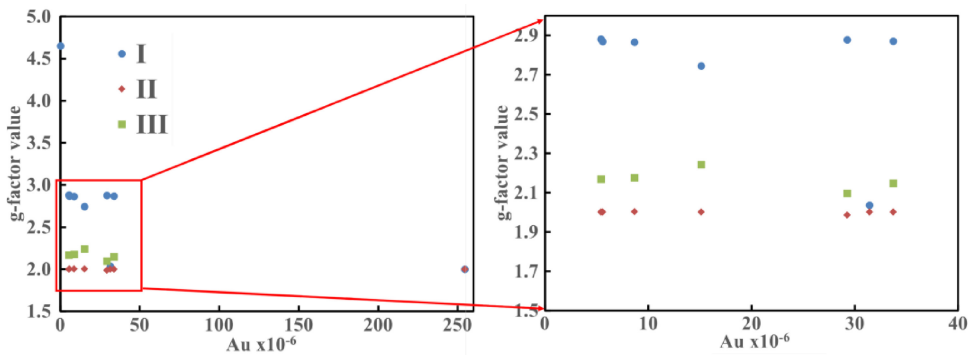

Fig. 14 *g* Factor values of various EPR absorption peaks of the pyrites

determined that with varying gold content in pyrite, the positions of the three typical absorption peaks γ_1, γ_2, and γ_3 change to varying degrees accordingly. Generally, with an increase in gold content in pyrite samples, γ_1, γ_2, and γ_3 tend to shift to higher wavenumbers (Fig. 15).

- The gold content in pyrite samples has a positive correlation with their relative absorbance (Table 8). The purpose of the concept of relative absorbance is to eliminate potential changes in the absolute absorbance resulting from slight differences in sample mass.

11 Discussion and conclusions

Through the study of both the physical and chemical typomorphic characteristics of pyrites from representative gold deposits in the study area, this paper concludes the following conclusions:

Pyrite grain size has a negative correlation with its gold content: coarse-grained euhedral pyrite has lower gold content than fine-grained subhedral and/or allotriomorphic pyrite; cubic pyrite, as the dominant crystal form, contains more gold than pentagonal dodecahedral pyrite in the area.

Both pyrite crystal forms and chemical compositions show that the replacement style of gold deposit formed in low saturability, low sulfur fugacity, and at temperatures either much higher or much lower than its best forming temperature, while that of the quartz vein style of gold deposit occurred under conditions with the best temperature, rich in sulfur and with high sulfur fugacity.

Au/Ag ratios in pyrites show that both the replacement and quartz vein styles of gold deposits are mesothermal and hypothermal. The Co/Ni ratios in the pyrites indicate that the quartz vein-style deposit is of magmatic-hydrothermal origin, while both the replacement and alkaline intrusive rock-related styles of gold deposits are not. The Co/Ni ratios of pyrites from all three styles of gold deposits have a generally negative correlation with gold content, possibly

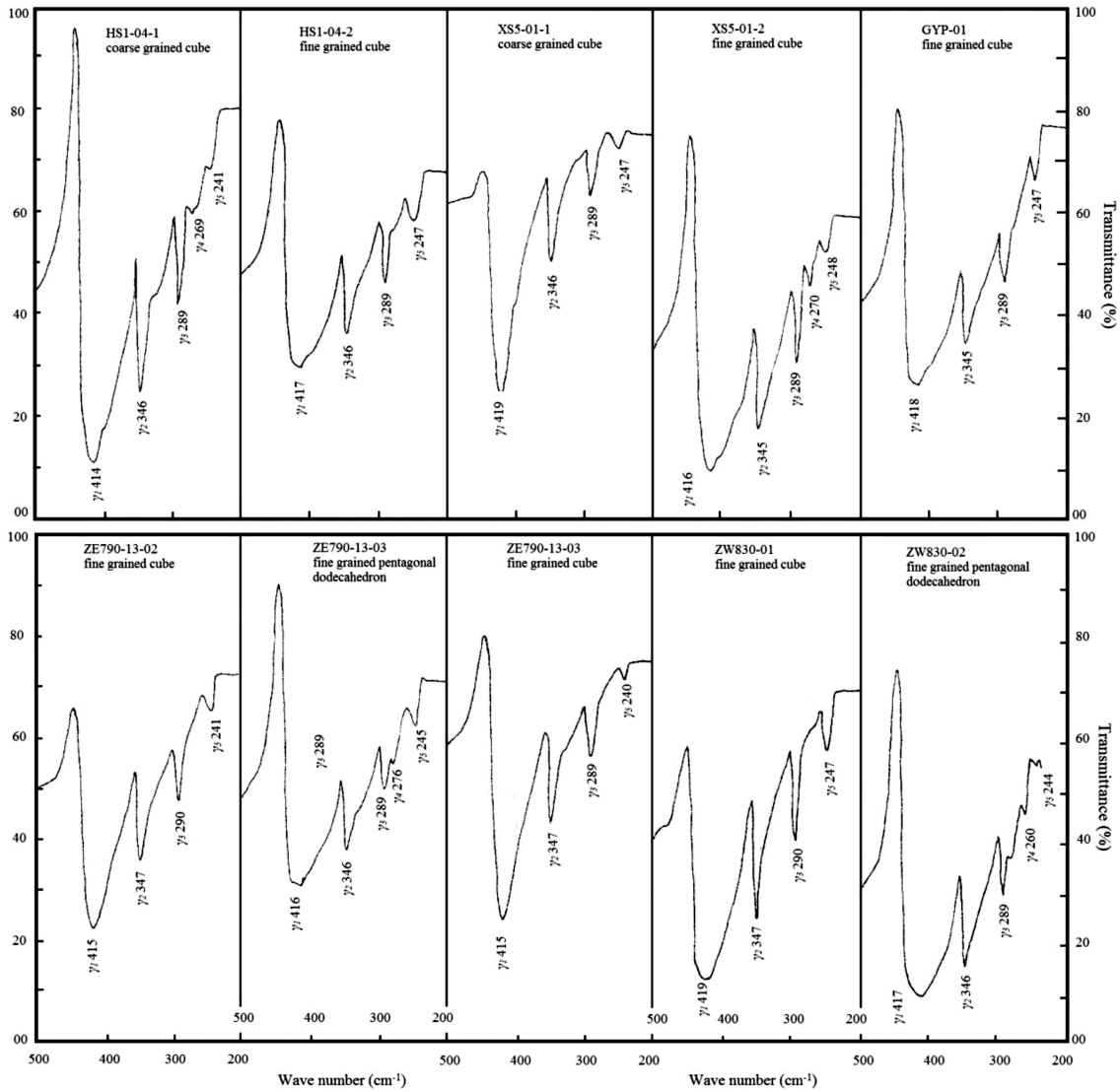

Fig. 15 Infrared absorption spectrum of pyrites from representative gold deposits

meaning that ore-forming materials were abyssal. Se/Te & S/Se ratios in pyrites from the replacement style of deposit indicate that it has nothing to do with the magmatic solution, which is consistent with that of the Co/Ni ratio, while that of the quartz vein style of deposit possibly indicates its hydrothermal solution was from multiple sources in addition to a magmatic origin.

Both the average α_0 and v_0 of pyrites from the Zhangquanzhuang deposit are greater than those from the Xiaoyingpan deposit, possibly meaning that both the poor and rich sulfide ore types and the metallogenic conditions of the two styles of gold deposits are different from each other to some degree. The X-ray diffraction intensity of pyrite rich in gold is lower than that of pyrite poor in gold from the Zhangquanzhuang deposit. In general, with an increase in gold content in pyrite, the total sum intensity ΣI decreases. Pyrite rich in gold usually contains higher Au, Ag, Co, Ni, As, Se, and Te, which results in lattice plane net defects when these trace elements enter pyrite, and the defects in turn result in lattice defect scattering when X-rays irradiate the plane net with defects and decrease the X-ray intensity.

Table 8 ISA results of pyrites from the representative mines

Gold mine	Series #	Sample #	Style	APN[(a)]	SAPF[(b)]	Absorbance (*Di*)					Relative absorbance				Au
					cm^{-1}	D_1	D_2	D_3	D_4	D_5	D_2/D_1	D_3/D_1	D_4/D_1	D_5/D_1	$\times 10^{-6}$
Xiaoyingpan	1	HS1-04-1	cg cube	5	414, 346, 289, 269, 241	0.8820	0.3299	0.1667	0.0602	0.0516	0.3740	0.1890	0.0680	0.0590	–
	2	HS1-04-2	fg cube	4	417, 346, 289, 248	0.3738	0.1615	0.1178	–	0.0558	0.4320	0.3150	–	0.1490	33.71
	3	XS5-01-1	fg cube	5	416, 345, 289, 270, 248	0.7907	0.3473	0.2076	0.7510	0.0471	0.4390	0.2630	0.0950	0.0600	15.11
	4	XS5-01-2	cg cube	4	419, 346, 289, 247	0.4452	0.1584	0.0709	–	0.0262	0.3560	0.1590	–	0.0590	–
Zhangquanzhuang	5	ZE790-13-02	fg cube	4	415, 347, 290, 241	0.4576	0.1818	0.1284	–	0.0389	0.3970	0.2810	–	0.0850	5.57
	6	ZE790-13-03	fg PD	5	416, 346, 289, 276, 245	0.4721	0.1537	0.1049	0.0706	0.0567	0.3260	0.2220	0.1500	0.1200	8.65
	7	ZE790-19-01	fg cube	4	415, 347, 289, 240	0.4890	0.1661	0.0938	–	0.0198	0.3400	0.1920	–	0.0400	–
	8	ZW830-01	fg cube	4	419, 347, 290, 247	0.7482	0.2993	0.1761	–	0.0691	0.4000	0.2350	–	0.0920	–
	9	ZW830-02	fg PD	5	417, 346, 289, 260, 244	0.7924	0.3651	0.2159	0.0824	0.0108	0.4610	0.2720	0.1040	0.0140	–
	10	CYP-01	fg cube	4	418, 345, 289, 247	0.4812	0.1660	0.1455	–	0.0593	0.3600	0.3150	–	0.1290	–

Analysis by the ISA lab, China University of Geosciences (Beijing)

cg, Coarse grained; fg, Fine grained; PD, Pentagonal dodecahedron

[(a)]Absorption peak number

[(b)]Signature absorption peak frequency

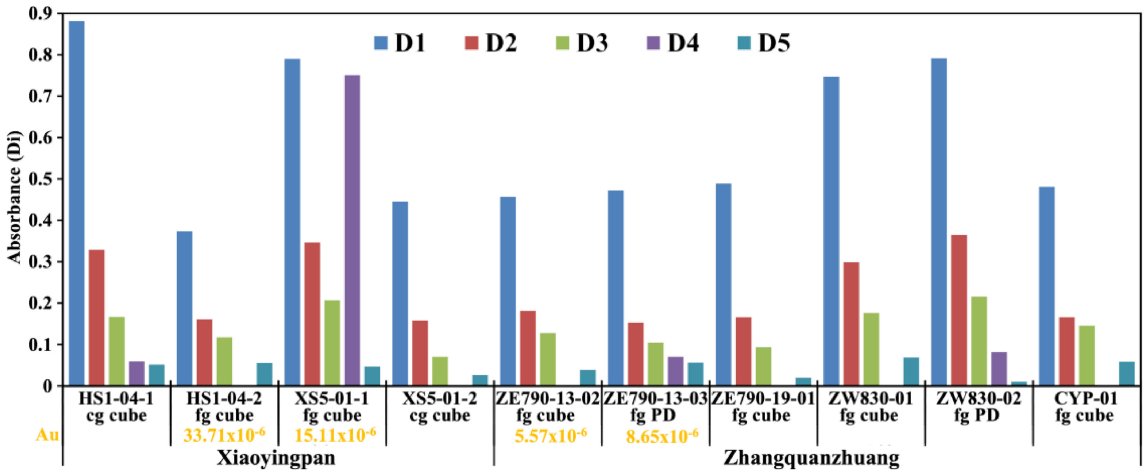

Fig. 16 ISA absorbance (*Di*) comparison of pyrites from representative gold deposits

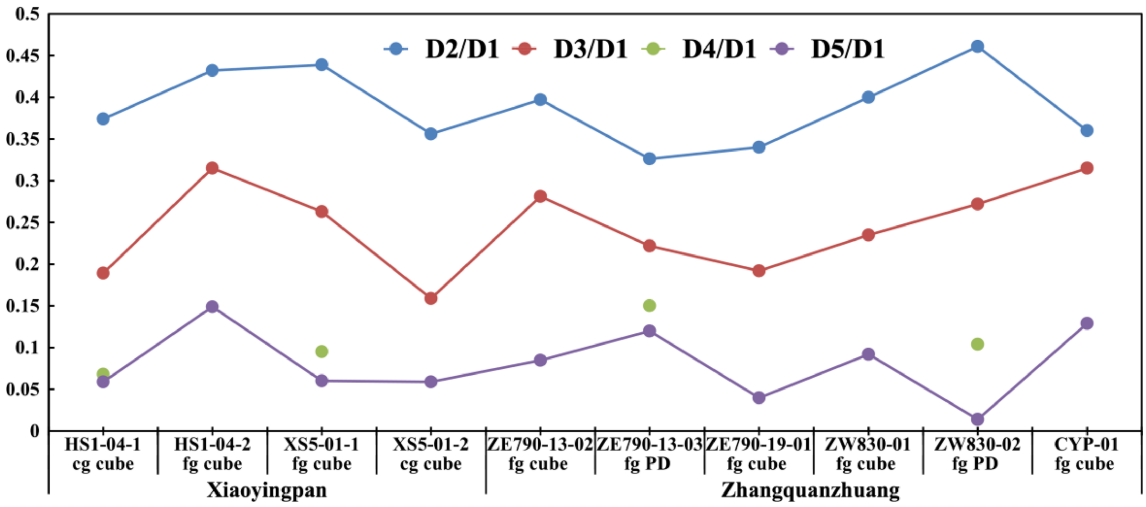

Fig. 17 ISA relative absorbance (Di/D_1) comparison of pyrites from representative gold deposits

The pyroelectricity coefficient has a negative correlation trend with the values of (Co + Ni + Se + Te)-As and (Co + Ni + Se + Te)/As. Pyrite pyroelectricity does not have any regular relationships with either its crystal form or gold content. The pyrite pyroelectricity of the Xiaoyingpan deposit is N-type, indicating that it formed under low sulfur fugacity, while that of the Zhangquanzhuang deposit is a mixture of P-N type, indicating that it formed under high sulfur fugacity. Meanwhile, pyrite pyroelectricity shows that the formation of the Xiaoyingpan deposit has something to do with metamorphism, while that of the Zhangquanzhuang deposit has to do with hydrothermal superposition. Comprehensively considering the ore control structures, host rocks, and other geological controls of the two styles of gold deposits, it is probable that the current mining level of the former mine is the root part of whole ore bodies, while that of the latter is the middle part of the total ore bodies. As a result, the ore-hunting target for the Xiaoyingpan mine is not at depth but instead along strike around the present mining site, while that for the Zhangquanzhuang mine is both at depth and along strike around the current mining site. On the pyroelectricity-temperature diagram, pyrite of the Xiaoyingpan deposit is mainly distributed between 200 and 270 °C, while pyrite of the Zhangquanzhuang deposit is distributed within 90–118 °C and 274–386 °C, demonstrating a multistage formation process.

In contrast to previous researchers' conclusions, the EPR test confirms the existence of lattice gold in pyrites from gold deposits in the study area. This provides

metallurgists with solid evidence to increase the gold milling recovery of ores in the study area. Au, in the form of Au^{+}, entering pyrite as an isomorph and producing electron–hole centers, makes the centers produce spin resonance absorption and results in EPR absorption peak II. The intensity of absorption peak II of auriferous pyrite has certain direct positive correlations with the gold content in pyrites. The #I and #III absorption peaks of the pyrites possibly result from the existence of Ni^{2+} and/or Cu^{2+}.

γ_1, γ_2, and γ_3 are the strongest and most typical absorption peaks of the infrared spectra of pyrites. The intensity, highest base intensity, wavenumbers, and intensity ratio of the corresponding absorption peaks of different samples are different from each other. Generally, with the increase in gold content in pyrite samples, γ_1, γ_2, and γ_3 tend to shift to higher wavenumbers. The gold content in the pyrite samples has a positive correlation with their relative absorbance.

Acknowledgements Support for this study was received from the China National Ph.D. Foundations and from Prof. Yusheng Zhai of China University of Geosciences, also an Academician of the Chinese Academy of Sciences, and from Prof. Zhaolu Pan and Jianhong Zhang of China University of Geosciences in Beijing, who provided insightful discussions and critical reviews of this manuscript. The chemical analyses, electron microprobe tests, X-ray diffraction, pyroelectricity tests, and infrared spectroscopic analyses of the pyrites were carried out at the labs of the China University of Geosciences in Beijing, while the EPR test was performed in the lab of the Department of Physics, Peking University, China. The authors very much appreciate the time invested by Mr. S. Daly, P. Geo of APEGBC, Canada; Mr. M. Storey, M. Eng. and P. Eng. with APEGBC of Canada and by David Yin, BSc of USA, for their review and editorial work on this contribution.

Author contributions The entire study included in the paper was proposed and organized by JY and SY, who should be regarded as co-first authors. Many of the figures and tables were prepared by HY, HS, JS, YC, and SX, who also helped the two co-first authors with the whole research. HS and SX helped complete the chemical analyses of this study. All authors prepared and reviewed the manuscript and approved the final version. Conceptualization, JY; Investigation, JY, SY, HY, HS, YC, and SX; Project administration, SY, HY, HS, YC, and SX; Writing—original draft, JY and JS.

Data availability The data that support the findings of this study is available from the authors upon reasonable request.

Declarations

Conflict of interest The authors declare that they have no conflict of interest.

References

Adams SS, and Putnam III BR (1992) Application of mineral deposit models in exploration: a case study of sediment-hosted gold deposits, Great Basin, western United States. In: Case histories and methods in mineral resource evaluation. Geological Society, Special Publication Number 63, pp 1–23

Arehart GB (1996) Characteristics and origin of sediment-hosted disseminated gold deposits: a review. Ore Geol Rev 11:383–403

Azzaman MA, Idrus A, Titisari AD (2021) Geology, hydrothermal alteration and mineralization of the Carlin-type gold deposit at South Ratatotok, Southeast Minahasa Regency, North Sulawesi Province, Indonesia. In: IOP conference series: Earth and environmental science, pp 1–9. https://doi.org/10.1088/1755-1315/789/1/012076

Barton MD, Seedorff E, Ilchik RP (1997) Contrasting siliceous replacement mineralization. Society of Economic Geologists, Society of Economic Geologists Guidebook Series. East-Central Nevada. https://doi.org/10.5382/GB.28

Chao Y, Yin J, Yin Y, Shi H, Xiang S (2022a) Occurrence state and properties of gold minerals from the gold deposits on the North China platform. European J Appl Sci. https://doi.org/10.14738/aivp.105.13292.10(5)2022,504-513

Chao Y, Yin J, Yin Y, Xiang S, Shi H, Wang J (2022b) The paragenetic stage of the Dongping gold deposit in the northern margin of the North China Platform. Eur J Appl Sci. https://doi.org/10.14738/aivp.106.13391.10(6)2022,38-47

Chen G (1987) Minerageny and prospecting mineralogy. Chongqing Publishing House, Chongqing (**in Chinese**)

Dang J (1991) The application of EPR spectra of quartz to the evaluation of gold ore deposits. Acta Petrologica et Mineralogica 10(1):68–73 (**in Chinese with English abstract**)

Dong J (1989) Genesis of gold deposits in the northern Hebei & western Liaoning Provinces, China. Geol Prospect 9:22–23 (**in Chinese with English abstract**)

Gao M (1991) Geochemistry of the Archean granulite facies metamorphic rocks in the Zhangjiakou-Xuanhua region, China. Geol Prospect 9:16–22 (**in Chinese with English abstract**)

Garwin SL, Hendri D, Lauricella PF (1995) The geology of the Mesel sediment-hosted gold deposit, North Sulawesi, Indonesia. In: Proceedings of the PACRIM congress 1995. Australian Institute of Mining and Metallurgy, pp 221–226

Hu D (1993) The significance of electron and hole centers in the assessment of gold deposits. Acta Petrologica et Mineralogica 12(4):356–362 (**in Chinese with English abstract**)

Hu X, Zhao J, Li S (1990) Gold mineralization in the Archean metamorphic rocks in the Zhangjiakou-Xuanhua region, China. J Tianjin Inst Geol Miner 22:2–9 (**in Chinese with English abstract**)

Jin S, Li H (1985) Brief introduction to minerageny. Jilin University Publishing House, Changchun (**in Chinese**)

Jones RS, Fleischer M (1969) Gold in minerals and the composition of native gold. Geological Survey Circular 612, United States Department of the Interior, pp 1–17

Kingston SP (2009) Nature and origin of gold-rich carbonate replacement deposits at the Rau occurrence, central Yukon. A thesis submitted in partial fulfilment of the requirements for the degree of bachelor of (geological) science (honours). This thesis conforms to the required standard. Supervisor: the University of British Columbia, Vancouver, BC

Li R (1992) Geology, geochemistry and metallogenic model of the Hougou gold deposit in Hebei Province, China. Geol Prospect 3:46–50 (**in Chinese with English abstract**)

Liu C (1997) The application of EPR and infrared spectra of quartz to the prospecting and evaluating of gold deposit in the middle Jiangxi province of China. J East China Geol Inst 20(4):313–318 (**in Chinese with English abstract**)

Lobato LMM, Vieira FWR (1998) Styles of hydrothermal styles of alteration and gold mineralization associated with the Nova Lima group of the QUADRILÁTERO FERRÍFERO: PART II, The Archean Mesothermal gold-bearing hydrothermal system. Revista Brasileira De Geociências 28(3):355–366

Percival TJP, Radtke AS, Bagby WM (1990) Relationships among Carbonate-Replacement Gold Deposits, Gold Skarns, and Intrusive Rocks, Bau Mining District, Sarawak. Malaysia. Min Geol 40(1):1–16

Poulsen KH, Robert F, Dubé B (2000) Geological classification of canadian gold deposits. Geol Surv Can Bull 540:1–113

Ravenelle JF (2013) Amphibolite facies gold mineralization: an example from the Roberto deposit, Eleonore property, James Bay, Quebec. Thèse. Québec, Université du Québec, Institut national de la recherche scientifique, Doctorat en sciences de la terre

Roberts, RJ (1986) The Carlin story. In: Tingley JV, Bonham Jr HF (eds) Sediment-hosted precious metal deposits of Northern Nevada. Nevada Bureau of Mines and Geology, Report 40, pp 71–80

Shao J (1990) Prospecting mineralogy of gold deposits. China University of Geosciences Publishing House, Wuhan (**in Chinese**)

Sillitoe RH (2020) Carlin-type and distal-disseminated gold deposits: A carbonate-replacement deposit perspective. In: October 2020 conference: vision for discovery. Geology and ore deposits of the basin and range. Geological Society of Nevada, Reno

Sillitoe RH, Bonham HF Jr (1990) Sediment-hosted gold deposits: distal products of magmatic-hydrothermal systems. Geology 18:157–161

Song R, Wang Y, Wang Z (1994) Geology of the lode gold deposits in Hebei Province, China. Geological Publishing House, Beijing (**in Chinese**)

Valette MDSS, Mercier-Langevin P, Côté-Mantha O, Simard M, Wodicka N, McNicoll VJ, Barbe P (2020) Lithological and tectonic controls on banded iron formation-associated gold at the Amaruq deposit, Churchill Province, Nunavut, and implications for exploration. Targeted Geoscience Initiative 5: contributions to the understanding of Canadian gold systems. Geological Survey of Canada, Open File 8712, pp 251–266. https://doi.org/10.4095/326042

Wang S (1986) Genetic research of the gold deposits in the Zhangjiakou-Xuanhua region, China. J Peking Univ (Nat Sci Ed) 4:81–89 (**in Chinese with English abstract**)

Wang H, Chen S (1996) Characteristics of the EPR spectra of quartz from the Heilongtan gold deposit in Suizhou, Hubei Province of China. Hubei Geol 10(1):75–78 (**in Chinese with English abstract**)

Wang J, Yin J, Chao Y, Yin Y, Xiang S, Shi H (2022) Structural control of gold deposits in the northern margin of the North China Platform. Eur J Appl Sci. https://doi.org/10.14738/aivp.106.13390.10(6)2022,29-37

Xiang S (1991) Preliminary research on the geology of the Hougou-type gold deposit. Geol Prospect 3:15–20 (**in Chinese with English abstract**)

Xu H, Liang R, Zhao J, Yang Y, Liang Y (2014) Geological characteristics of the gold triangle region and its prospecting target, Hebei Province, China. Miner Explor 5(1):14–20 (**in Chinese with English abstract**)

Yin J, Shi H (1995) Geology of the gold deposits in the Zhangjiakou-Xuanhua Region China. Geological Publishing House, Beijing, pp 42–59 (**in Chinese with English abstract**)

Yin J, Zhai Y (1994) Metallogenic series of gold deposits in the Zhangjiakou-Xuanhua region of Hebei Province, China. J Guilin Coll Geoly 14(4):359–369 (**in Chinese with English abstract**)

Yin J, Liu Y, Shi H (2021) Chemical and physical characteristics of quartz from gold deposits in the North China platform: relationship to gold mineralization. Acta Geochimica 40(6):998–1022. https://doi.org/10.1007/s11631-021-00487-x

Zhang Q (1984) Geology and metallogeny of the early Precambrian in China. Jilin People's Publishing House, Changchun (**in Chinese with English abstract**)

Zheng Y (1990) Structural research on the Dongping gold deposit in Chongli County, Hebei Province, China. Geol Prospect Rev 2:20–27 (**in Chinese with English abstract**)